BMFPs, a versatile therapeutic tool for redirecting a preexisting Epstein-Barr virus antibody response toward defined target cells

Benoît Gamain, Carine Brousse, Nathan E Rainey, Béré K Diallo, Clara-Eva Paquereau, Alexandra Desrames, Jolita Ceputyte, Jean-Philippe Semblat, Olivier Bertrand, Stéphane Gangnard, et al.

HEALTH AND MEDICINE

BMFPs, a versatile therapeutic tool for redirecting a preexisting Epstein-Barr virus antibody response toward defined target cells

Benoît Gamain[1], Carine Brousse[1], Nathan E. Rainey[1], Béré K. Diallo[2], Clara-Eva Paquereau[1], Alexandra Desrames[1], Jolita Ceputyte[1], Jean-Philippe Semblat[1], Olivier Bertrand[1], Stéphane Gangnard[1], Jean-Luc Teillaud[2], Arnaud Chêne[1]*

Industrial production of therapeutic monoclonal antibodies is mostly performed in eukaryotic-based systems, allowing posttranslational modifications mandatory for their functional activity. The resulting elevated product cost limits therapy access to some patients. To address this limitation, we conceptualized a novel immunotherapeutic approach to redirect a preexisting polyclonal antibody response against Epstein-Barr virus (EBV) toward defined target cells. We engineered and expressed in bacteria bimodular fusion proteins (BMFPs) comprising an Fc-deficient binding moiety targeting an antigen expressed at the surface of a target cell, fused to the EBV-P18 antigen, which recruits circulating endogenous anti-P18 IgG in EBV$^+$ individuals. Opsonization of BMFP-coated targets efficiently triggered antibody-mediated clearing effector mechanisms. When assessed in a P18-primed mouse tumor model, therapy performed with an anti-huCD20 BMFP significantly led to increased survival and total cancer remission in some animals. These results indicate that BMFPs could represent potent and useful therapeutic molecules to treat a number of diseases.

INTRODUCTION

The generation of therapeutic monoclonal antibodies (mAbs) is a tedious process, which requires integrating the complex structural and biochemical features of the immunoglobulin (Ig) molecules to achieve the desired effector functions and exhibit optimal in vivo efficacy (*1*, *2*). Over the past decades, mAbs developed to deplete target cells, such as tumor cells or normal autoimmune cells, for instance, B cells in multiple sclerosis, have drawn a particular attention, and substantial efforts have been undertaken to engineer Ig with optimized biological activity and improved pharmacokinetic properties (*3*, *4*). Fc-mutated and glyco-engineered IgG have been developed to maximize their potential to trigger complement-dependent cytotoxicity (CDC) (*5*, *6*), antibody-dependent cell-mediated cytotoxicity (ADCC) (*7*–*10*), and antibody-dependent phagocytosis (*11*). Engineering of the Fc region of IgG has also permitted to modulate the pH-dependent affinity of some antibodies for neonate Fc receptors, consequently modifying the mAb pharmacokinetic properties and enhancing in vivo half-life (*12*, *13*).

The vast majority of mAbs are repeatedly injected at high doses to achieve significant therapeutic effects (*14*). mAb production has, therefore, to be performed at a very large scale. Today, most therapeutic mAbs are expressed in eukaryotic cell–based systems, allowing the production of large quantities of functional proteins presenting proper posttranslational modifications, such as glycosylation. However, such systems require arduous selection processes and long production cycles, resulting in increased mAb manufacturing cost. Thus, the development of mAb-based therapies presents substantial hurdles and remains challenging, in particular, when long-term iterative treatments are needed.

We envisioned the possibility of generating bimodular fusion proteins (BMFPs) able to redirect polyclonal endogenous high-affinity antibodies produced by plasma cells derived from memory B cells against Epstein-Barr virus (EBV) toward defined target cells. BMFPs could then be designed on the basis of an EBV antigen module fused to a specific ligand (binding moiety) targeting a protein of interest on the surface of a target cell. BMFPs could circumvent the need for all the complex engineering studies aiming at improving the effector functions of a single mAb and allow the use of diverse ligand units devoid of Fc chains, such as nanobodies (Nbs), to trigger Fcγ-dependent effector mechanisms by recruiting anti-EBV polyclonal antibodies exhibiting a large spectrum of functions and produced over long periods of time in individuals.

EBV is a ubiquitous human herpes virus 4 that infects more than 95% of the adult population worldwide (*15*). Following primary infection, EBV establishes a life-long persistent infection, residing in a latent stage in memory B cells (*16*). The persistence of the virus results from a fine balance between viral latency, viral replication, and host immune responses (*17*). Consequently, infected individuals have, all along their life, antibodies directed against various EBV antigens including the conserved small capsomere-interacting protein P18 [open reading frame (ORF) BFRF3] (fig. S1), which is predominantly recognized by antibodies belonging to the IgG1 subclass (*18*). This human IgG subclass is the most commonly used for therapeutic antibodies, whatever their formats (chimeric, humanized, or fully human mAbs) (*19*), as it triggers and regulates immune effector mechanisms via the binding of the Fcγ region to the complement component C1q (*20*, *21*) and to Fcγ receptors (FcγRs) present at the surface of a broad range of leukocyte subpopulations (*22*, *23*). It also triggers proinflammatory or anti-inflammatory processes depending on the sialylation on the N-linked glycan of the Fc region (*24*). Thus, a P18-containing fusion molecule with a

[1]Université de Paris, Biologie Intégrée du Globule Rouge, UMR_S1134, INSERM, F-75015 Paris, France. [2]Laboratory "Immune Microenvironment and Immunotherapy", INSERM U.1135, Centre d'Immunologie et des Maladies Infectieuses (CIMI-Paris), Faculté de Médecine, Sorbonne Université, 91 boulevard de l'Hôpital, 75013 Paris, France.
*Corresponding author. Email: arnaud.chene@inserm.fr

predefined binding specificity could allow the recruitment of endogenous anti-P18 IgG1 antibodies at the surface of target cells and then trigger Fc-dependent and complement-dependent immune effector mechanisms (Fig. 1). Expressible in bacteria-based systems, P18-based BMFPs could be produced at a low manufacturing cost as compared to current therapeutic mAbs, offering broader access to patients.

To establish a proof of concept that P18-based BMFPs could display efficient biological activity and potentially represent a universal and versatile platform to develop novel therapeutics against a broad range of diseases, we based our study on two different models, developed sequentially, in which the nature of the BMFP binding moiety varies. The first model, in which P18-derived antigens are fused to an Nb directed against human red blood cells (RBCs) (Fig. 1, model 1), was used as a screening model to select for the most efficient P18 fragment to promote anti-EBV antibody recruitment. Furthermore, this model was chosen for its relative simplicity to deploy and because of the availability of an Nb directed against an RBC antigen. Using this model, we could identify a P18 fragment (P18F3) presenting optimal properties to serve as a specific IgG-recruiting antigen. Once the most efficient P18-derived fragment was selected, a second model was developed to assess the effectiveness of a BMFP in a preclinical setting. The selected P18F3 peptide was therefore fused to a single-chain variable fragment (scFv) directed against the human cluster of differentiation 20 (huCD20) expressed on most mature B cells, which represents an exquisite target for antibody-based therapy of B cell–related diseases (Fig. 1, model 2). The ability of this anti-huCD20 BMFP to trigger B cell depletion through the recruitment of preexisting anti-P18 antibodies was assessed in various in vitro assays. An in vivo mouse tumor model, previously developed to explore the vaccinal effect of anti-tumor antibodies (*25*, *26*), was also used to evaluate the antitumor capacity of the anti-huCD20 BMFP when injected into mice having anti-P18 antibodies.

We show here that functional BMFPs, carrying binding moieties of different natures and targeting human RBCs and huCD20$^+$ cells, efficiently bind to their respective cellular targets and recruit anti-P18 antibodies at the cell surface, triggering efficient immune effector functions. A strong in vitro RBC phagocytosis by macrophage-like cells derived from FcγRI$^+$/RIIa$^+$ monocytic leukemia THP1 cells was detected when using an anti-DARC BMFP in combination with IgG present in the plasma of EBV$^+$ individuals. We also show that in vitro treatment of huCD20$^+$ Burkitt's lymphoma cells with an anti-huCD20 BMFP elicits a significant activation of the antibody-dependent complement cascade and triggers FcγRIII-mediated activation of the nuclear factor of activated T cell (NFAT) pathway in an ADCC reporter assay in the presence of plasma containing anti-P18 antibodies. Last, we show an increased survival of P18-preimmunized immunocompetent mice bearing huCD20$^+$ tumor cells following anti-huCD20 BMFP treatment. Together, these results indicate that BMFPs are versatile tools for redirecting a preexisting EBV immune antibody response toward predefined target cells and could represent potent and useful therapeutic molecules in patients.

RESULTS

Engineering BMFPs against DARC

Duffy antigen receptor for chemokines (DARC), also known as Fy glycoprotein, is a promiscuous chemokine receptor abundantly present at the surface of RBCs from individuals carrying the FY^{a+}/FY^{b+},

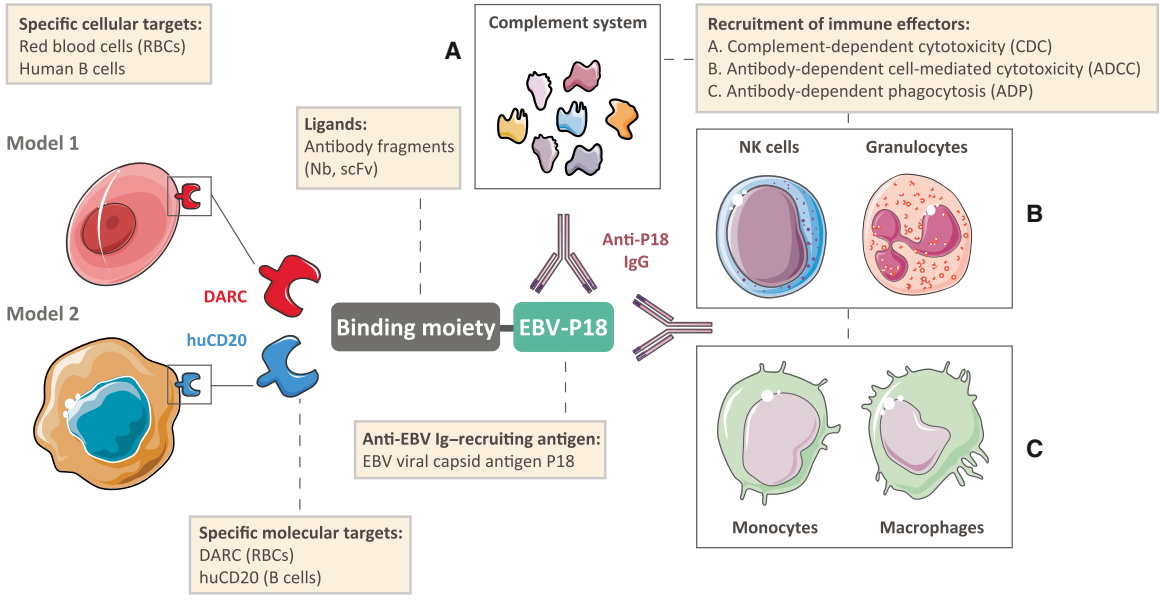

Fig. 1. Conceptual modes of action of BMFPs. The EBV-P18 antigen is bound by circulating anti-EBV IgG present in the plasma of individuals chronically infected by EBV. Once fused to a binding moiety specifically directed to a molecule expressed by the targeted cells, P18 can serve as a recruiting agent for endogenous anti-P18 IgG and mediate their opsonization. The subsequent triggering of antibody-dependent effector mechanisms, i.e., complement activation via Fcγ binding to the complement component C1q (**A**) and/or ADCC and phagocytosis by immune cells expressing FcγRs (**B** and **C**), ultimately leads to the elimination of the target cells. Target cells and relevant target molecules developed in the two models assessed in this study are depicted. DARC, Duffy antigen receptor for chemokines; huCD20, human cluster of differentiation 20. The art pieces used in the figure were obtained from Servier Medical Art by Servier, licensed under a Creative Commons Attribution 3.0 Unported License (https://smart.servier.com/) and modified.

FY^{a-}/FY^{b+}, or FY^{a+}/FY^{b-} genotypes (*27*) and was therefore considered as a molecular target of choice to generate a first set of BMFPs targeting human erythrocytes in a proof-of-concept model (Fig. 1, model 1). To generate anti-DARC BMFPs, we chose an Nb targeting the extracellular domain 1 (ECD1), which specifically binds to $DARC^+$ human RBCs with high affinity (*28*). The CA52 anti-DARC Nb (Nb-αDARC) was genetically fused to the N-terminal part of full-length P18 (P18FL). Protein sequence analysis of P18FL revealed that its N-terminal part displays several stretches of hydrophobic residues and numerous prolines that could potentially interfere with the expression of stable proteins in physiological buffers (Fig. 2A). Furthermore, P18FL displays a cysteine at position 56 (Cys^{56}) that could unwillingly engage in disulfide bond formation with other cysteines present within the binding moiety sequence during folding of the fusion constructs, as antibody fragments have structuring disulfide bonds mandatory for their functionality and stability. To overcome these potential issues, we designed P18 fragments lacking the N-terminal region that contains Cys^{56}. The sequence delimitations of the three P18-derived fragments (P18F2, P18F3, and P18F4) were chosen with regard to the boundaries of hydrophobic cluster regions within the whole protein (Fig. 2, A and B).

The resulting recombinant constructs were expressed in *Escherichia coli* SHuffle bacteria, which allow disulfide bond formation within the cytoplasm (see the BMFP production scheme in fig. S2) (*29*). Soluble nonaggregated Nb-αDARC-P18F2, Nb-αDARC-P18F3, Nb-αDARC-P18F4, and Nb-αDARC could be purified (>95%) by size exclusion chromatography (Fig. 2, C and D) in large amounts (≈5 mg $liter^{-1}$ of culture) and used for subsequent experiments. In contrast, the protein solubility of Nb-αDARC-P18FL was poor and led to extensive aggregation during purification, preventing its further use (Fig. 2C).

The biochemical and functional properties of Nb-αDARC and P18-derived polypeptides were then sequentially examined. Nb-αDARC, Nb-αDARC-P18F2, Nb-αDARC-P18F3, and Nb-αDARC-P18F4 were first subjected to surface plasmon resonance (SPR) analysis to determine their affinity constants for their cognate molecular target, DARC. The extracellular domain of DARC (DARC-ECD1) and the CA52 epitope-mutated form of this domain (DARC-ECD1-Mut), which is no longer recognized by the anti-DARC Nb (fig. S3), were expressed in *E. coli* as fusion proteins with glutathione *S*-transferase (GST), purified (Fig. 2E), and then immobilized on the reference and analytical channels (Fc1 and Fc2, respectively) of a CM5 chip. Sensorgrams are shown in Fig. 2F. The fitted kinetic data derived from the sensorgrams revealed that the fusion of P18-derived polypeptides to Nb-αDARC did not markedly modify the affinity (K_d constants ranging from 2.75×10^{-11} M to 7.42×10^{-11} M) of the Nb binding moiety for its target as compared to Nb-αDARC alone ($K_d = 9.00 \times 10^{-11}$ M) (Fig. 2F). Notably, the values of the k_{off} and k_{on} constants of Nb-αDARC-P18F2 markedly differed from those of the two other BMFPs and of Nb-αDARC, as shown by a lack of clusterization around Nb-αDARC in the RaPID plot shown in Fig. 2G.

The capacity of the BMFPs to be bound by IgG present in the plasma of EBV^+ individuals was then assessed. P18FL, which serves as a reference for IgG binding, was expressed in *E. coli* as a maltose-binding protein fusion (MBP-P18FL) to ensure appropriate solubility (Fig. 2H, left). Enzyme-linked immunosorbent assay (ELISA) performed with 22 individual plasma samples revealed that the binding levels of circulating IgG to Nb-αDARC-P18F2 and Nb-αDARC-P18F3 were similar to those of the P18FL. Statistical analysis showed that IgG bound to Nb-αDARC-P18F2 and Nb-αDARC-P18F3 to the same extent. IgG binding to the Nb-αDARC-P18F4 was noticeably lower, although the differences with αDARC-P18F2 and Nb-αDARC-P18F3 did not reach statistical significance (Fig. 2H, right). No binding to Nb-αDARC or to MBP was observed.

Overall, these results positioned P18F3 as the shortest P18-derived polypeptide bound by anti-P18 IgG to the same extent as the P18FL, with no major change in the specificity and affinity of the Nb-αDARC moiety of this BMFP for its cognate target. Nb-αDARC-P18F3 was therefore selected for further functional investigations. We then reasoned that BMFP treatment efficacy would most likely rely on anti-P18F3 antibody titers. To assess the relationship between BMFP-mediated triggering of effector mechanisms in vitro and the amount of anti-P18F3 antibodies present in the plasma, we generated three plasma pools presenting different anti-P18F3 antibody titers toward P18F3. These pools were defined on the basis of the distribution of optical density at 655 nm (OD_{655nm}) values of individual plasma samples obtained by an ELISA performed to determine the binding of each sample to P18F3 (Fig. 2H). We then used a quantile-based approach for dividing the samples into three different intervals containing the same number of samples ($n = 7$ in each group). Seven plasma samples demonstrating the lowest IgG titers toward P18F3 (red dots) composed the plasma pool termed "low," seven plasma samples demonstrating intermediate IgG titers toward P18F3 (dark blue dots) composed the plasma pool termed "inter," and seven plasma samples demonstrating the highest IgG titers toward P18F3 (light blue dots) composed the plasma pool termed "high." The only plasma sample binding to both MBP and Nb-αDARC alone (white dot) was excluded from pooling. The distribution of the samples within each group is presented in fig. S4A and the anti-P18F3 IgG titers of each pool in fig. S4B.

Nb-αDARC-P18F3 binds to native DARC and recruits endogenous anti-EBV IgG to the RBC surface

The interaction of IgG present in human plasma pools, presenting different antibody titers against the EBV-derived antigen P18F3, with Nb-αDARC-P18F3 bound to native DARC expressed at the surface of $DARC^+$ RBCs (former genotype FY^{a+}/FY^{b+}) was then assessed by flow cytometry (Fig. 3). An indirect anti–His-tag fluorescence assay showed first that the fusion of the P18F3 peptide to the C-terminal part of the Nb-αDARC did not prevent the resulting BMFP from binding to RBCs, although a higher concentration was needed to reach the binding plateau as compared to Nb-αDARC (fig. S5). In the presence of human plasma pools exhibiting low, intermediate, and high antibody titers against P18F3, the binding of Nb-αDARC-P18F3 to $DARC^+$ RBCs led to the recruitment of anti-P18 IgG and hence to opsonization of the target cells (Fig. 3A and fig. S6). The binding amplitude of IgG was in line with the anti-P18F3 antibody titers found in the human plasma pools (fig. S4B), as detected by an indirect immunofluorescence assay (Fig. 3A). No noticeable recruitment of IgG was observed when RBCs were incubated with Nb-αDARC regardless of the plasma pools tested. A qualitative analysis performed by confocal microscopy confirmed that the fluorescence signal resulting from Nb-αDARC-P18F3–mediated IgG recruitment was located at the cell surface of RBCs (Fig. 3, B and C).

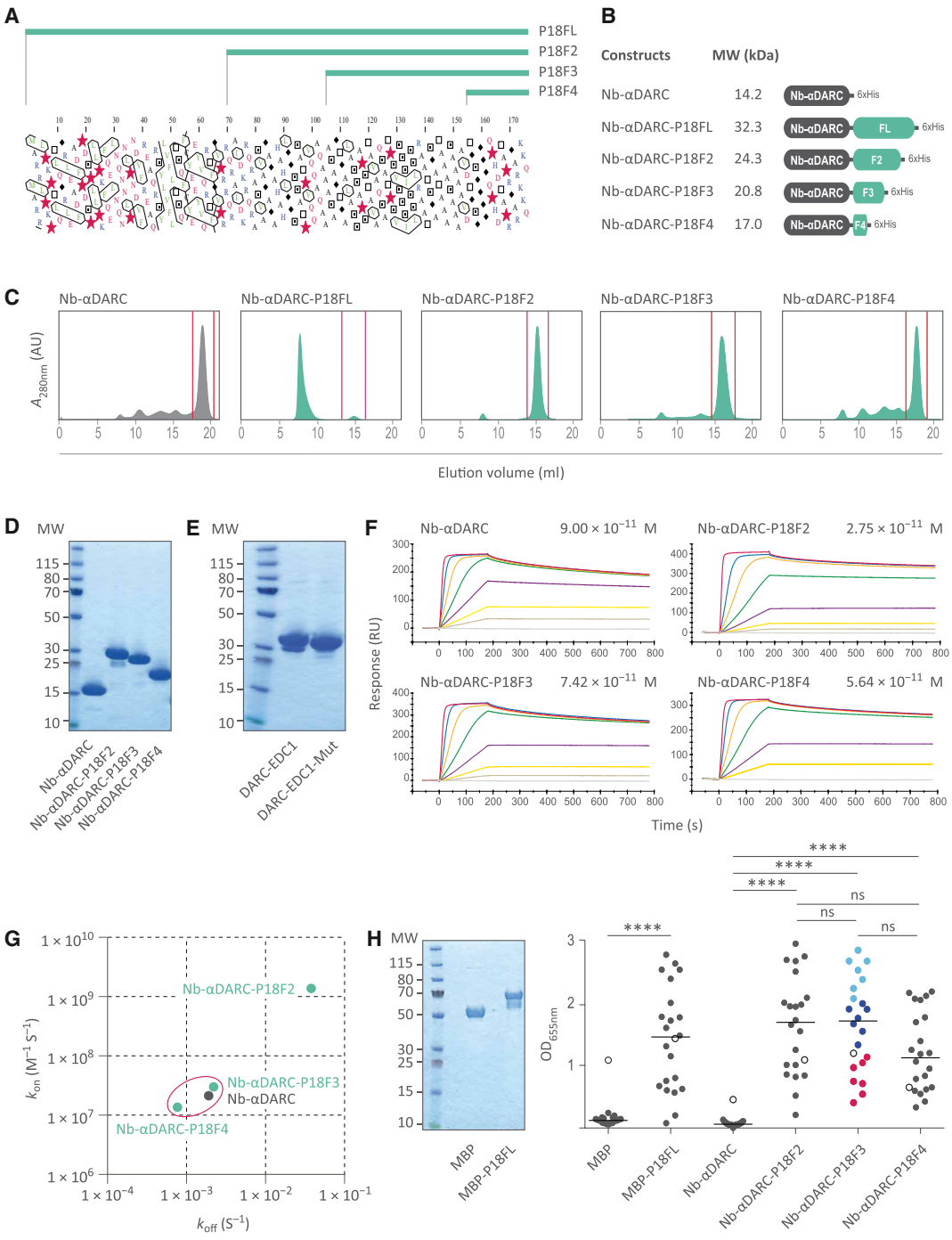

Fig. 2. Engineering BMFPs against DARC. (**A**) Hydrophobic cluster analysis plot of P18. Strong hydrophobic amino acids are encircled, and their contours are joined, forming clusters (HCA 1.0.2, Ressource Parisienne en BioInformatique Structurale). (**B**) Architecture of BMFPs comprising an Nb targeting DARC and P18 fragments of different lengths. MW, molecular weight. (**C**) Gel filtration profiles of Nb-αDARC and Nb-DARC-P18 BMFPs. Red bars delimit the protein of interest (POI) pick. AU, arbitrary units. (**D**) SDS–polyacrylamide gel electrophoresis (SDS-PAGE) analysis of eluted POIs (Coomassie). (**E**) SDS-PAGE analysis of GST fusion proteins DARC-ECD1 and DARC-ECD1-Mut. (**F**) SPR analysis of the interactions between immobilized DARC and αDARC-P18 BMFPs. Calculated K_d values are displayed. M, molars; RU, response units. (**G**) RaPID plot resulting from SPR analysis. Calculated k_{on} and k_{off} values are plotted. Nb-αDARC-P18F3 and Nb-αDARC-P18F4 cluster around Nb-αDARC within the red circle. (**H**) Left: SDS-PAGE analysis of MBP-P18FL. Right: Binding of IgG present in plasma samples (1/100 dilution) from 22 EBV^+ individuals to αDARC-P18 BMFPs. Group comparison between MBP and MBP-P18FL was performed using the Mann-Whitney test. Multiple group comparison between Nb-αDARC, Nb-αDARC-P18F2, Nb-αDARC-P18F3, and Nb-αDARC-P18F4 was performed using the Dunn's multiple comparison test. ns, nonstatistically significant. Seven plasma samples displaying low, intermediate, or high binding levels to Nb-αDARC-P18F3 (red, dark blue, and light blue dots, respectively) were mixed to obtain three different pools (low, inter, and high).

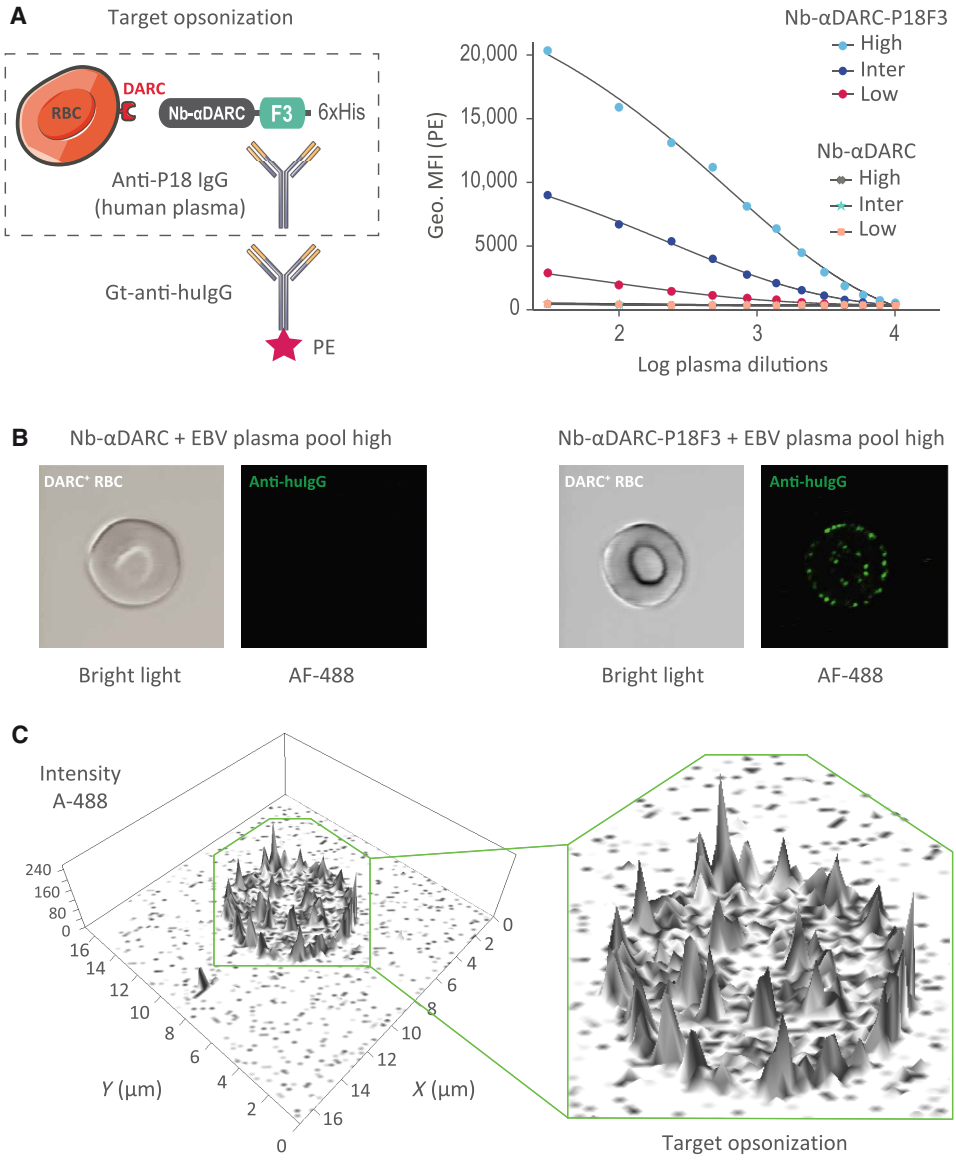

Fig. 3. Nb-αDARC-P18F3 binds to native DARC and recruits anti-EBV huIgG to the RBC surface, promoting target opsonization. (**A**) The ability of Nb-αDARC-P18F3 to promote RBC opsonization by IgG present in the human plasma pools exhibiting different antibody titers against P18F3 was assessed by an indirect immunofluorescence assay and flow cytometry. Nb-αDARC and Nb-α DARC-P18F3 were used at a concentration that results in a similar binding to RBCs, 9.6 nM (fig. S5). Membrane-bound huIgG was detected using anti-huIgG antibodies conjugated to phycoerythrin (PE). Plotted data represent the mean values of duplicates. MFI, mean fluorescence intensity. (**B**) A qualitative analysis was performed by confocal microscopy to confirm that the signal resulting from huIgG detection was localized at the RBC surface. Confocal laser scanning microscopy images of huIgG distribution on the RBC membrane after incubation of RBCs with Nb-αDARC or Nb-αDARC-P18F3 in the presence of plasma exhibiting a high antibody titer to P18F3 (right of each pair). The binding of huIgG was revealed with goat Alexa Fluor 488 anti-huIgG antibodies (indicated as A-488). (**C**) Representation in 2.5D of the A-488 signal obtained when RBCs were incubated with Nb-α DARC-P18F3 in the presence of plasma exhibiting a high antibody titer to P18F3. The right inset shows the enlarged 2.5D representation. Fluorescence is located at the RBC surface. Because of the biconcave shape of RBCs, membrane fluorescence located within the cell structure on the scanning microscopy images must not be mistakenly interpreted as cytosolic fluorescence. Confocal microscopy was performed with a Zeiss LSM700 microscope, and images were analyzed with ZEN 2.0 software. AF-488, Alexa Fluor 488.

Nb-αDARC-P18F3–mediated RBC opsonization triggers erythrophagocytosis by macrophage-like THP1 cells

Engagement of FcγRI (CD64), FcγRIIa (CD32a), and FcγRIIIa (CD16a) present on monocytes and macrophages promotes phagocytosis of IgG-opsonized target cells (*30*). Thus, to assess whether anti-P18F3 huIgG recruited by Nb-αDARC-P18F3 bound to DARC$^+$ RBCs were able to promote RBC clearance by phagocytes, we performed an erythrophagocytosis assay using macrophage-like cells derived from the monocytic leukemia THP1 cell line (CD64$^+$/CD32a$^+$/CD16a$^-$) (fig. S7) (*31*). Carboxyfluorescein succinimidyl ester (CFSE)–stained DARC$^+$ RBCs were incubated for 3 hours at 37°C with macrophage-like cells [obtained by phorbol 12-myristate 13-acetate (PMA) treatment of THP1 cells] in the presence of Nb-αDARC-P18F3 and of human plasma pools exhibiting low,

intermediate, or high antibody titers against P18F3. Flow cytometry analysis of macrophage-like THP1 cells revealed that the percentage of CFSE$^+$ THP1 was largely increased when the cells were incubated with Nb-αDARC-P18F3 and a human plasma pool exhibiting a high titer of anti-P18F3 antibodies (Fig. 4A). When Nb-αDARC was used instead of Nb-αDARC-P18F3, no significant increase was observed (Fig. 4A). Four independent experiments confirmed that exposure of RBCs to Nb-αDARC-P18F3 and human plasma pools containing high or intermediate antibody titers against P18 provokes an increased erythrophagocytosis by THP1-derived macrophage-like cells (mean fold change of 6.3 and 2.6, respectively), as compared to the condition using untreated RBCs (Fig. 4B). No increase was observed in the absence of plasma in the assay where Nb-αDARC-P18F3 was used (Fig. 4B). Notably, erythrophagocytosis was more pronounced in the presence of the plasma pool exhibiting the highest antibody titer against P18F3 (as compared to the "no plasma" condition; Dunn's multiple comparison test, $P = 0.028$). In contrast, RBC treatment with Nb-αDARC did not modify the level of erythrophagocytosis directly exerted by macrophage-like THP1 cells, regardless of the plasma pools tested (Fig. *4*B).

Together, these results identified P18F3 as the most efficient P18-derived polypeptide able to recruit specific IgG onto the surface of target cells. Fusion of P18F3 to an Nb-based binding moiety (Nb-αDARC) did not alter the intrinsic functionality of the two modules and demonstrated a good capability to recruit anti-P18 antibodies present in human plasma, which engaged FcγRs on THP1-derived macrophages, leading to the triggering of RBC phagocytosis.

Engineering a BMFP against human CD20

We then developed a BMFP containing a scFv directed against huCD20 fused to the N-terminal end of P18F3 to target Burkitt's lymphoma cells in vitro and huCD20-expressing tumor cells in an in vivo mouse tumor model. An anti-huCD20 scFv comprising the variable region of immunoglobulin heavy chain (V_H) domain fused to the variable region of immunoglobulin light chain (V_L) domain [with a $(GGGGS)_3$ interdomain linker] derived from the mouse IgG2b, κ 2H7 mAb (*32*) was engineered (Fig. 5A) and expressed alone ($scFv_{2H7}$) or in fusion with P18F3 ($scFv_{2H7}$-P18F3) (Fig. 5B and fig. S8). Both constructs included a 6xHistidine (6xHis) tag at the C terminus. The binding of the $scFv_{2H7}$ and $scFv_{2H7}$-P18F3 to native huCD20 expressed at the surface of cells from the Burkitt lymphoma cell line RAJI (fig. S9A) was assessed by an indirect anti–His-tag fluorescence assay and flow cytometry (fig. S9B). Both $scFv_{2H7}$ and $scFv_{2H7}$-P18F3 bound to huCD20-expressing RAJI cells, and a similar binding was observed when used at an equimolar concentration of 0.48 μM. As already observed with Nb-αDARC and Nb-αDARC-P18F3 (fig. S5), a difference in the binding curves of the two molecules was observed (fig. S9B). This may reflect a steric hindrance for the binding of the anti-6xHis antibody to the recombinant molecules when P18F3 is fused at their C terminus rather than a change in the ability of BMFPs to bind the target molecules (DARC and huCD20).

$ScFv_{2H7}$-P18F3–mediated anti-P18 IgG opsonization of Burkitt's lymphoma cells activates the antibody-dependent complement cascade and triggers FcγRIIIa-mediated activation of intracellular signaling pathways

We then evaluated whether the binding of $scFv_{2H7}$-P18F3 to Burkitt's lymphoma cells induced the activation of the complement cascade in the presence of a pool of human plasma exhibiting a high titer of anti-P18F3 antibodies. This activation leads to the formation of the C5b-8 complex that binds to C9 to form the membrane

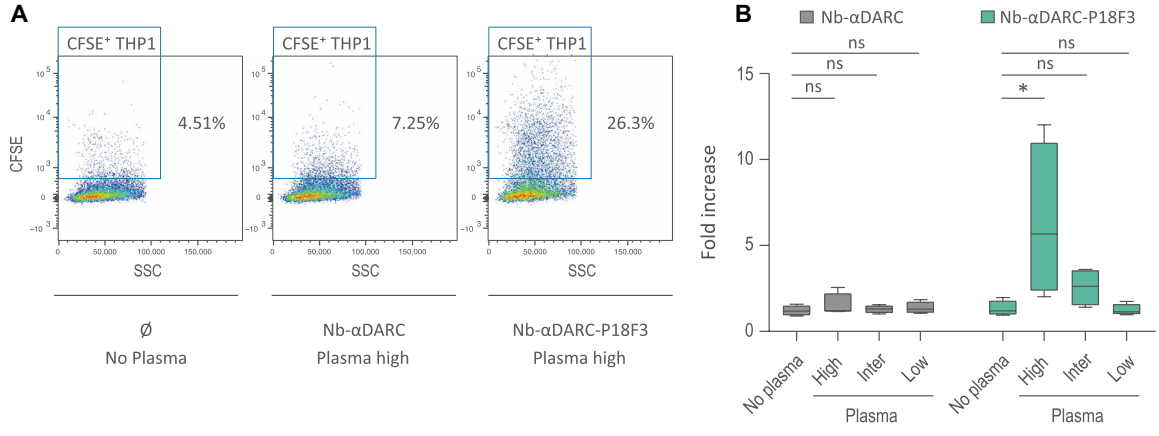

Fig. 4. Nb-αDARC-P18F3–mediated RBC opsonization triggers erythrophagocytosis by macrophage-like THP1 cells. The ability of Nb-αDARC-P18F3 to promote RBC phagocytosis by THP1-derived macrophages was assessed in an erythrophagocytosis assay. CFSE-stained DARC$^+$ RBCs were first incubated with Nb-αDARC or Nb-αDARC-P18F3 and with plasma pools exhibiting different antibody titers to P18F3. Following a 3-hour culture with THP1-derived macrophages, nonphagocytized RBCs were lysed, and THP1 cells were then subjected to immunofluorescence analysis. (**A**) Representative data obtained from one experiment. A CFSE$^+$ THP1 cell was regarded as a cell having phagocytized at least one RBC. Untreated cells (left) served as a reference for basal erythrophagocytosis by macrophage-like THP1-derived cells. Nb-αDARC-P18F3 treatment of RBCs in the presence of plasma exhibiting a high antibody titer against P18 (indicated plasma high) led to a marked increase in the percentage of CFSE$^+$ THP1 cells (right) as compared to Nb-αDARC–treated RBCs (middle). CFSE$^+$ THP1 represents CFSE$^+$ macrophage-like THP1-derived cells. SSC, side scatter. (**B**) Results obtained from four independent experiments are expressed as a fold increase (ordinate) in the percentage of CFSE$^+$ macrophage-like THP1-derived cells incubated with RBCs coated with Nb-αDARC or Nb-αDARC-P18F3 and plasma pools exhibiting different antibody titers to P18F3 (high, intermediate, and low) compared to the percentage of CFSE$^+$ cells incubated with untreated RBCs (i.e., no incubation with Nb-αDARC or Nb-αDARC-P18F3 and no plasma). Box plots include the mean horizontal line and interquartile range (box), whereas the whiskers represent the minimal and maximal values. For both treatments (Nb-αDARC and Nb-αDARC-P18F3), group comparisons between the condition without plasma and the conditions with plasma high, intermediate, and low were performed using the Dunn's multiple comparison test.

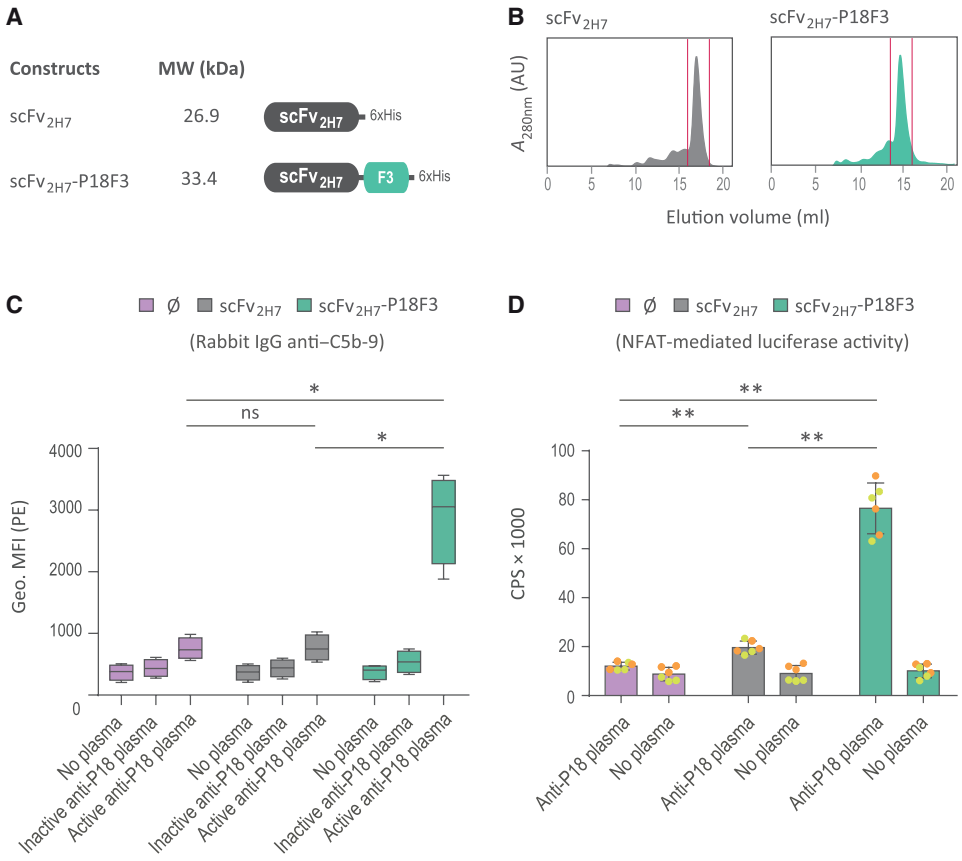

Fig. 5. $ScFv_{2H7}$-P18F3–mediated opsonization of Burkitt's lymphoma cells induces activation of the antibody-dependent complement cascade and triggers FcγRIIIa-mediated activation of intracellular signaling pathways that leads to ADCC. (**A**) Architecture $scFv_{2H7}$-P18F3 and of $scFv_{2H7}$ targeting huCD20. (**B**) Gel filtration profiles of $scFv_{2H7}$ and $scFv_{2H7}$-P18F3. Red bars delimit the protein of interest pick. (**C**) The capability of $scFv_{2H7}$-P18F3 to promote complement activation through the classical pathway (antibody-dependent) was assessed by monitoring the deposition of the MAC C5b-9 at the surface of RAJI cells. Results obtained from four independent experiments are depicted. Box plots include the mean horizontal line and interquartile range (box), whereas the whiskers represent the minimal and maximal values. Ø, no scFv protein. Group comparison was performed using the Mann-Whitney test. (**D**) The capability of $scFv_{2H7}$-P18F3 to promote early events that lead to ADCC was assessed using a reporter assay. Activation of gene transcription through the NFAT pathway was quantified in engineered Jurkat cells using a luciferase assay. CPS, counts per second. Results obtained from two independent experiments (orange and yellow circles) performed in triplicates are depicted. Boxes represent the mean values of the six measurements, and the error bars depict the associated SDs. Group comparison was performed using the Mann-Whitney test.

attack complex (MAC), C5b-9. Incubation of RAJI cells with $scFv_{2H7}$-P18F3 in the presence of plasma led to more C5b-8/9 deposition than when untreated cells or cells coated with $scFv_{2H7}$ were tested, as shown by an increased detection of C5b-8/9 using either rabbit anti–C5b-9 antibodies (Fig. 5C) or a mouse anti–C5b-8/9 mAb (fig. S10A).

The Fcγ region of immuno-complexed IgG can bind to FcγRIIIa/CD16a expressed at the surface of natural killer (NK) cells and trigger an intracellular signaling cascade, leading to the release of interferon-γ, tumor necrosis factor–α, and perforin and granzymes from cytotoxic granules. Thus, we examined whether $scFv_{2H7}$-P18F3–mediated anti-P18 IgG opsonization of Burkitt's lymphoma cells could engage FcγRIIIa, hence triggering a signaling cascade that ultimately leads to ADCC. Jurkat cells stably expressing human FcγRIIIa-V158, which binds IgG1 more efficiently than FcγRIIIa-F158, were used as effector cells to monitor cell activation. In this reporter assay, FcγRIIIa engagement by immune complexes transduces intracellular signals, resulting in NFAT-mediated luciferase activity, which represents a robust and valid downstream readout for ADCC induction by IgG1 antibodies (*33*). Thus, $huCD20^+$ RAJI cells were first coated with $scFv_{2H7}$-P18F3 or $scFv_{2H7}$ and then cocultured with $FcγRIIIa^+$ Jurkat cells in the presence of a pool of plasma exhibiting a high titer of anti-P18F3 antibodies for 6 hours. Treatment of RAJI cells with $scFv_{2H7}$-P18F3 markedly increased NFAT-mediated luciferase activity in Jurkat cells in the presence of plasma as compared to untreated cells or $scFv_{2H7}$-coated cells (Fig. 5D and fig. S10B), demonstrating that P18F3-mediated anti-P18 IgG opsonization of Burkitt's lymphoma cells triggers FcγRIIIa-mediated activation of intracellular signaling pathways that leads to ADCC.

Treatment with $scFv_{2H7}$-P18F3 reduces cancer progression in mice bearing $huCD20^+$ tumor cells

First, to raise mouse antibodies directed against P18F3, 12 BALB/cByJ mice were immunized with the P18FL protein fused to MBP (MBP-P18FL). Analysis of IgG subclasses 52 days after the first injection revealed that around 46.8% of anti-P18F3 IgG are IgG1 and 34.9% IgG2b (mean values) (fig. S11). A smaller proportion of anti-P18 IgG belonged to the IgG3 and IgG2a subclasses (10.4 and 7.9%, respectively) (mean values). Individual preimmune and immune sera from the 12 mice were then used to perform an opsonization

assay with EL4–wild-type (WT) cells and transduced EL4-huCD20 cells that stably express human CD20 (*34*) (fig. S12A). In the presence of immune mouse sera, binding of $scFv_{2H7}$-P18F3 to EL4-huCD20 cells led to the recruitment of anti-P18 mouse IgG, as detected by an immunofluorescence assay using specific goat anti-mouse IgG (Fc-specific) antibodies conjugated to allophycocyanin (APC), and hence to opsonization of target cells (Fig. 6A). No noticeable recruitment of IgG was observed in the absence of scFv (Fig. 6A), when the $scFv_{2H7}$ was tested (Fig. 6A) and when EL4-WT was treated with $scFv_{2H7}$ or $scFv_{2H7}$-P18F3 and incubated with preimmune sera (fig. S12B).

Second, to determine whether $scFv_{2H7}$-P18F3 therapy can protect mice from tumor challenge, C57Bl/6 immunocompetent mice were immunized with MBP-P18FL to generate endogenous anti-P18 antibodies (Fig. 6B). Mice were then injected intravenously with 2.5×10^5 EL4-huCD20 cells (day 0) and received $scFv_{2H7}$-P18F3 therapy (group G1.1), consisting of four intraperitoneal injections at days 1, 4, 7, and 10. In a first set of experiments, three additional control groups ($n = 5$) were injected with tumor cells. Mice from group G1.2 were left untreated, whereas mice from group G1.3 received four injections of $scFv_{2H7}$. Mice from group G1.4 received $scFv_{2H7}$-P18F3 therapy but were not preimmunized with MBP-P18FL (Fig. 6C). All mice from G1.2, G1.3, and G1.4 died within 35 to 50 days after tumor cell injection. In contrast, the overall long-term survival in the G1.1 group ($scFv_{2H7}$-P18F3 therapy) was 40% (Fig. 6C). In a second set of experiments involving a larger number of animals, two groups were designed. Animals from the G2.1 group ($n = 12$) received $scFv_{2H7}$-P18F3 therapy, whereas mice from the G2.2 group ($n = 11$) did not receive any treatment after injection of tumor cells (Fig. 6D). All mice from the untreated group died before day 60 (median survival of 35 days). $ScFv_{2H7}$-P18F3 therapy significantly increased mice survival (median survival of 51.5 days; log-rank Mantel-Cox test, $P = 0.0387$) and led to an overall 17% long-term survival. Two days before EL4-huCD20 cell injection, most circulating anti-P18F3 IgG in mice from G1.1 and G2.1 belonged to the IgG1 and IgG2b subclasses (Fig. 6, C and D, right), as already observed in sera from MBP-P18FL–immunized mice used to test IgG opsonization (fig. S11). In addition, $scFv_{2H7}$-P18F3 treatment led to increased levels of circulating antibodies directed against P18F3 at day 15 after treatment (fig. S13).

DISCUSSION

Here, we describe a strategy for redirecting a preexisting EBV antibody response toward defined pathogenic cells using BMFPs comprising a specific binding moiety and an EBV-derived IgG antibody-recruiting antigen, P18. As a proof of concept, we first generated a set of BMFPs targeting RBCs via an anti-DARC Nb. This made it possible to select the most efficient P18 fragment to promote anti-EBV antibody recruitment and to show that treatment of RBCs with BMFPs in the presence of human plasma from EBV^+ donors mediated target opsonization by circulating anti-P18 IgG and the subsequent induction of erythrophagocytosis by macrophage-like cells. We then developed a scFv-based BMFP directed toward huCD20 ($scFv_{2H7}$-P18F3) and analyzed its efficacy in vitro and in vivo in a mouse tumor model. $ScFv_{2H7}$-P18F3–mediated opsonization of Burkitt's lymphoma cells activated the antibody-dependent cascade of the complement system and engaged FcγRIII in a cell assay, recapitulating the first steps of ADCC triggering. When assessed in a tumor model, $scFv_{2H7}$-P18F3 therapy significantly increased mice survival, leading to total cancer remission in some animals.

The initial part of this work consisted of establishing that BMFPs, expressed in a bacteria-based system, could be designed to efficiently target defined cellular elements. The conservation of the intrinsic biochemical and functional properties of both modules (P18 and binding moiety) is crucial when designing BMFPs aiming at redirecting a preexisting EBV antibody response toward specific cells. To create a versatile therapeutic tool, in which the binding moiety could be easily substituted, we first optimized the nature of the P18 antigen using a model targeting DARC expressed at the surface of RBCs with an Nb-based BMFP (Nb-αDARC). The EBV antigen P18 has been selected primarily for its capability to be strongly bound by circulating IgG from EBV-infected individuals (*18*). Another important criterion for selecting P18 was the absence of any posttranslational addition of sugar moieties. P18 is a non-glycosylated protein of small size (18 kDa) that could therefore be produced in a heterologous bacterial system. We used a mutant *E. coli* strain (SHuffle) that promotes disulfide bond formation in the cytoplasm, leading to more efficient folding of recombinant proteins, improved activity, and increased production yields (*29*). This cell line was recently used to produce a cysteine-rich malaria vaccine candidate that was then transitioned to a phase 1 clinical trial (*35*, *36*), demonstrating its potential to support large-scale production of proteins containing disulfide bonds. We also optimized the P18 antigen to efficiently recruit circulating anti-P18 IgG, without affecting the functionality of the binding moiety. P18F3 was down-selected as the prime P18-derived antigen, presenting binding titers by circulating anti-P18 IgG comparable to that of P18FL, thus confirming the presence of immunodominant epitopes within the C-terminal part of the protein (*37*). Notably, fusion of P18F3 to Nb-αDARC did not markedly affect the affinity of the Nb for its cognate target, DARC. Furthermore, RBC treatment with Nb-αDARC-P18F3 triggered erythrophagocytosis by THP1-derived macrophages. The amplitude of erythrophagocytosis correlated with the anti-P18F3 binding titers of the circulating IgG, strongly suggesting that erythrophagocytosis was driven by IgG opsonization rather than by pattern recognition receptors or mannose receptor engagement.

On the basis of these results, we then generated a P18F3-derived BMFP comprising a scFv binding moiety targeting huCD20 that is expressed at the surface of B lymphocytes from early developmental stages (late pro-B cell) to late stages (memory B cell) as well as in most non-Hodgkin's B lymphomas. mAb therapy targeting huCD20 has revolutionized the treatment of B cell malignancies for more than 30 years, becoming the leading therapeutic agents for the care of numerous B cell–related cancers such as follicular lymphoma, diffuse large B cell lymphoma, mantle cell lymphoma, and Burkitt's lymphoma (*38*). The most notable example of such success is rituximab (*39*). Several other therapeutic anti-huCD20 mAbs such as ofatumumab, obinutuzumab, and ublituximab [derived from the EMAB-6 antibody (*40*)] have been developed since the advent of rituximab (with alternate binding epitopes, additional humanization, and modified glycosylations) (*41*, *42*). We have developed here a binding moiety targeting the large extracellular loop of huCD20 based on the C2H7 (2H7) chimeric antibody, which presents a different binding epitope profile from rituximab (*43*). $ScFv_{2H7}$-P18F3 expression in SHuffle resulted in the production of a soluble protein, with a production yield (after purification) reaching 0.7 to

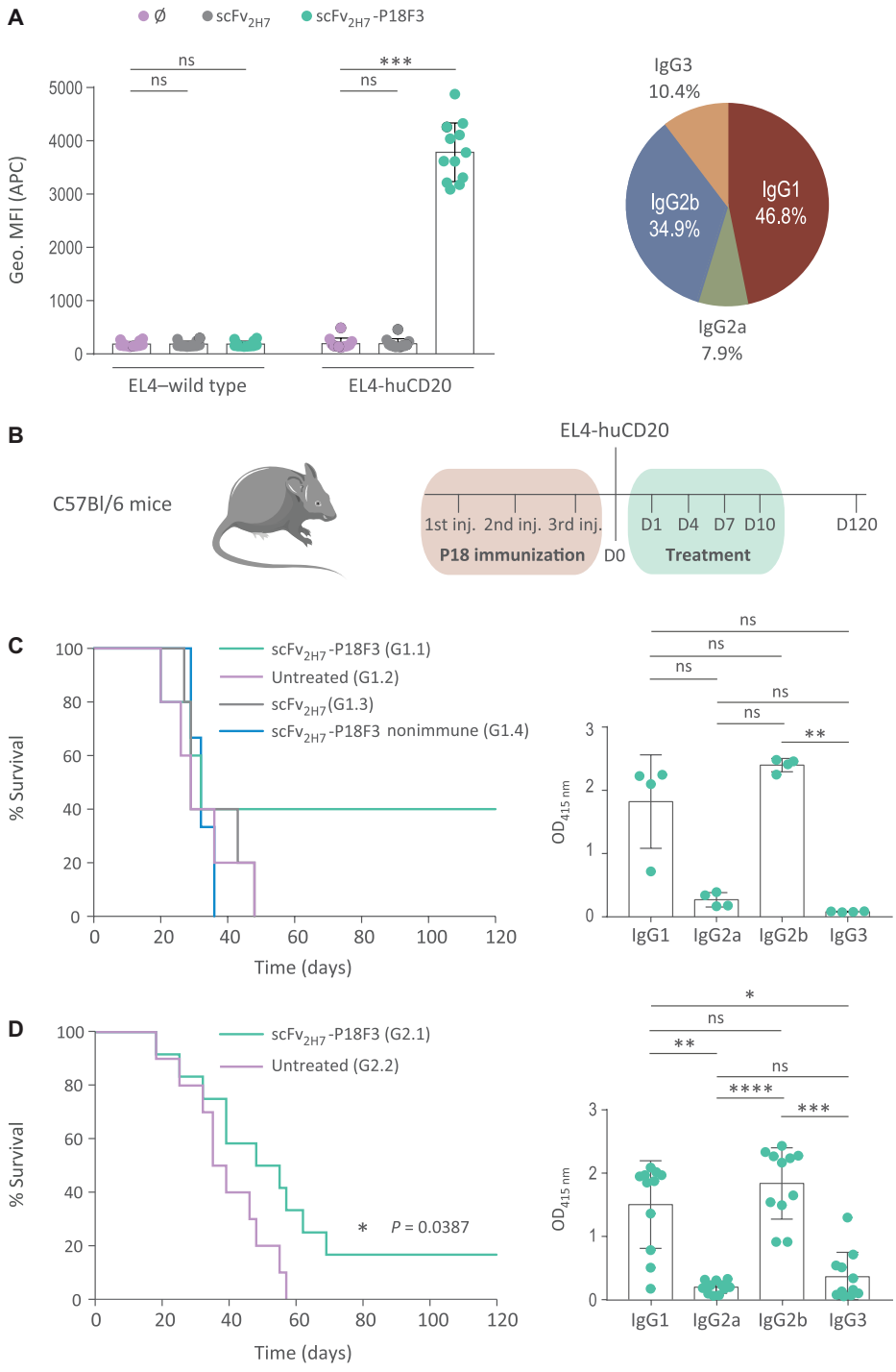

Fig. 6. Treatment with scFv$_{2H7}$-P18F3 reduces cancer progression in mice bearing EL4-huCD20 tumor cells. (**A**) Opsonization of scFv$_{2H7}$-P18F3–coated EL4-huCD20 cells by IgG present in the individual serum (1/10 dilution) of 12 BALB/cByJ mice immunized with MBP-P18FL. Group comparisons between the condition without protein and the conditions with scFv$_{2H7}$ and scFv$_{2H7}$-P18F3 were performed using the Dunn's multiple comparison test. The proportion of the different IgG subclasses present in the circulation of BALB/cByJ mice immunized with MBP-P18FL is displayed as a pie chart. (**B**) The antitumor effect of scFv$_{2H7}$-P18F3 therapy was assessed in a mouse tumor model. C57Bl/6 mice were preimmunized with MBP-P18FL. Mice were then injected with EL4-huCD20 cells at day 0 (D0) and received scFv$_{2H7}$-P18F3 therapy at days 1, 4, 7, and 10. (**C**) Left: Mice belonging to G1.1 and G.1.4 received scFv$_{2H7}$-P18F3 therapy, but mice from G.1.4 were not preimmunized with MBP-P18FL. Right: Anti-P18F3 IgG subclasses present in sera collected 2 days before EL4-huCD20 injection into G1.1 mice. (**D**) Left: Mice belonging to G2.1 ($n = 12$) received scFv$_{2H7}$-P18F3 therapy, whereas mice from G2.2 ($n = 11$) received PBS. Right: Anti-P18F3 IgG subclasses in sera collected 2 days before EL4-huCD20 injection into G2.1 mice. Comparison of survival curves was performed using the log-rank (Mantel-Cox) test ($\chi^2 = 4.275$). Multiple group comparisons between IgG subclasses were performed using the Dunn's multiple comparison test. The art pieces used in the figure are modified from Servier Medical Art by Servier, licensed under a Creative Commons Attribution 3.0 Unported License (https://smart.servier.com/).

1 mg liter^{-1} of bacteria culture, in line with previous work highlighting the difficulty to express stable and soluble scFv molecules (*44*, *45*). We can speculate that the use of antitumor Nbs as binding moieties in BMFPs might be more suitable for preclinical and clinical development than scFv, because Nbs can be produced at low cost in milligram quantities per liter of culture (*46*, *47*).

We demonstrate here that treatment of Burkitt's lymphoma cells with scFv$_{2H7}$-P18F3, in the presence of plasma from EBV$^+$ donors, activates the complement cascade, leading to the formation of the MAC as shown by the detection of C5b-9 deposition at the cell surface. The ability of the scFv$_{2H7}$-P18F3 to trigger the MAC formation and deposit on target cells strongly supports the relevance of BMFP-based treatments to deplete pathologic cells. Several in vivo studies have highlighted that complement activation is important for the therapeutic activity of depleting antibodies, as exemplified by anti-huCD20 mAbs (*34*, *48*). In addition to complement activation, scFv$_{2H7}$-P18F3–mediated opsonization also provoked the engagement of FcγRIII at the surface of engineered Jurkat cells in the presence of plasma from EBV$^+$ individuals, triggering the first steps of the signaling cascade leading to ADCC. Thus, these data indicate that anti-huCD20 BMFPs used in EBV$^+$ patients could enable the recruitment of endogenous anti-P18 IgG at the surface of huCD20$^+$ B cells, leading to the triggering of immune effector mechanisms. The continuous bioavailability of endogenous polyclonal IgG could represent a strong benefit to improve engagement of the C1q complement component and of FcγRs, thus leading to a sustained therapeutic efficacy.

The in vivo antitumor efficacy of scFv$_{2H7}$-P18F3 therapy was therefore assessed in a mouse model. Early attempts in the late 70s to develop in vivo EBV models by virus inoculation of nonhuman primates did not result in asymptomatic persistent infections (*49*). Since then, humanized mice, which can recapitulate key aspects of EBV infection observed in humans, have been established (*50*, *51*). However, these models are arduous to implement and still face some severe limitations including suboptimal IgG responses (*52*). To assess the antitumor activity of scFv$_{2H7}$-P18F3 in vivo in the presence of anti-P18 antibodies, we used a mouse tumor model, in which cells expressing human CD20 (EL4-huCD20) served as tumor target cells (*25*, *26*, *48*, *53*). Mice were first preimmunized with MBP-P18FL to generate circulating anti-P18F3 antibodies. Previous works (*25*, *26*) that used the same mouse tumor model required a cumulative dose of 1 mg (five injections at days 1, 4, 7, 10, and 13 of 200 μg) of an IgG2a anti-huCD20 mouse mAb, the most effective mouse subclass to engage FcγRs and to activate complement, to achieve antitumor efficacy. Our experimental design consisted of only four injections of scFv$_{2H7}$-P18F3 for a cumulative dose of 228 μg. The 57-μg dosage of scFv$_{2H7}$-P18F3 per injection was chosen here as it corresponds to the same number of therapeutic molecules contained in 200 μg of IgG2a. Following EL4-huCD20 injection, preimmunized mice that received scFv$_{2H7}$-P18F3 therapy showed a protection against tumor development as shown by an increased survival time and by the full tumor clearance observed in 17 to 40% of the animals. Analysis of the mouse IgG subclasses specific to P18F3 induced by MBP-P18FL immunization revealed a predominance of IgG1 and, to a slightly lower extent, of IgG2b. In contrast to human IgG1, mouse IgG1 is poorly able to bind C1q or to engage activating FcγRs. Conversely, this subclass can efficiently bind to the inhibitory FcγRIIb. Thus, it is important to stress that, despite these marked limitations, the efficacy of scFv$_{2H7}$-P18F3 therapy is achieved under less favorable conditions than in humans, where human IgG1, the major component of the anti-P18 antibody response, exhibits strong effector functions through the binding to C1q and to activating FcγRs. Using the same experimental setting (i.e., the intravenous injection of EL4-huCD20), we have previously shown that both the presence of NK cells and of an intact Fc region, as well as the activation of dendritic cells, are required for achieving a long-term antitumor protection by an anti-huCD20 IgG2a antibody treatment (*25*, *53*). Furthermore, DiLillo and Ravetch (*26*) have demonstrated, using also the same mouse model, that the antitumor effect of this IgG2a antibody and of a human IgG1 antibody (in the latter case, in transgenic mice expressing human FcγRs) is related to the recruitment of activating mouse and human FcγRs expressed by macrophages and dendritic cells. Thus, together, these works demonstrated that the antitumor protection of mice injected with EL4-huCD20 cells and treated with anti-CD20 antibodies is mediated through the engagement of FcγRs. The presence of IgG2b (about 35%) and IgG2a (about 8%), the only two mouse IgG subclasses that strongly bind mouse activating FcγRs (*54*) in the sera of MBP-P18FL–immunized mice, argues in favor of an efficient triggering of ADCC and phagocytosis participating to the antitumor protection of the animals.

Overall, our data suggest that the effectiveness of BMFP therapeutics is dependent not only on widespread EBV infection throughout the human population but also on titers of anti-P18F3 polyclonal antibodies present in circulation. The determination of the anti-P18F3 antibody threshold required for treatment efficacy in humans cannot be extrapolated from the results presented in this study performed in in vitro settings or in vivo using a model that does not properly reflect the immune response elicited in humans upon chronic EBV infection. This important consideration should therefore be thoroughly assessed in early clinical trials. Would the baseline of anti-P18F3 antibody titers make it difficult to trigger fully effective clearing mechanisms upon a first injection with BMFP therapeutics, this administration, eventually followed by iterative treatments, will trigger a rapid anti-P18 recall response, thanks to the pool of memory B cells present in treated patients. P18-stimulated memory B cells will differentiate into plasma cells producing large amounts of anti-P18F3 antibodies within a few hours/days. Note also that several diseases are accompanied by a reactivation of the EBV lytic cycle and by increased levels of circulating anti-EBV antibodies (*55*–*57*), thus creating a favorable context for BMFP therapy effectiveness. Notably, scFv$_{2H7}$-P18F3 treatment in the mouse EL4-huCD20 model allowed the recall of the P18F3 antibody response (fig. S13).

Alternative approaches using bispecific antibodies directed against T cells and tumor cells have been proven to be efficient in some hematologic malignancies such as relapsed/refractory B cell precursor acute lymphoblastic leukemia. However, these bispecific antibodies can cause serious side effects (severe, life-threatening, or leading to death). An overactivation of T cells provoking cytokine release syndrome has been documented for anti-CD3ε × anti-CD19 bispecific antibodies, such as blinatumomab. This T cell activation has also been associated with neurologic adverse events (neurological disorders, neutropenia, and sepsis). As of December 2018, a total of 3196 serious adverse drug reactions of 7102 patients exposed to blinatumomab have been reported (since its international marketing in December 2014) (*58*).

By contrast, BMFPs have important advantages over T cell engagers. By recruiting polyclonal anti-P18 IgG, BMFPs allow the

activation of numerous cells from innate immunity (NK cells, macrophages, and neutrophils) that express a variety of FcγRs (FcγRI, FcγRIIIa, and FcγRIIa) and induce ADCC and phagocytosis. They do not directly activate T cells, making cytokine storm unlikely as opposed to bispecific antibodies or antibodies that target activating surface T cell molecules (CD3ε and CD28). They can also induce a long-term adaptive antitumor protection by recruiting and activating dendritic cells that also express various activating FcγRs (*25*, *26*, *53*). The major isotype of anti-P18 antibodies (IgG1) made these antibodies also capable of activating the classical complement pathway. Last, the permanent presence of circulating anti-P18 antibodies, possibly accompanied by a rapid increase of anti-P18 titers due to the recall response after BMFP injection, could positively affect the pharmacokinetics/pharmacodynamics of the injected BMFP by stabilizing the complexes formed between anti-P18 antibodies and BMFP, leading to a long-lasting targeting of tumor cells.

Overall, our study shows that EBV-derived BMFPs could represent a versatile therapeutic tool for redirecting an EBV preexisting antibody response toward defined target cells. Their main advantages over the use of therapeutic depleting/cytotoxic mAbs are (i) the flexibility of the constructs in terms of binding moieties that can be easily made of antibody fragments with various specificities such as scFv, Nbs, or other types of ligands directed against a specific cell surface receptor; (ii) the lack of Fc region, rendering unnecessary any further Fc engineering for gaining optimized effector functions due to the recruitment of polyclonal anti-P18 IgG1 exhibiting excellent cytotoxic properties (CDC and ADCC); (iii) the reduced doses to be injected due to the recruitment of polyclonal endogenous IgG, mostly IgG1, directed against P18, a mechanism that will amplify the efficacy of antibody-mediated effector functions; (iv) a continuous bioavailability of endogenous polyclonal effector IgG; and (v) the ability to produce large amounts of BMFPs using bacteria and not eukaryotic cells, with reduced costs of production.

MATERIALS AND METHODS

Production and purification of MBP-P18FL, DARC-ECD1, and DARC-Mut

Genomic EBV DNA (strain B95-8) was isolated from cells of the marmoset (*Callithrix jacchus*) cell line B95-8 [European Collection of Authenticated Cell Cultures (ECACC)]. The complete DNA sequences of the ORF BFRF3 encoding for the viral capsid antigens (UniProt P14348; amino acids 1 to 176) were cloned into the pMal-C2x plasmid (New England Biolabs) suitable for expression of MBP fusions. The sequences coding for the DARC-ECD1 and the CA52 epitope-mutated form of this domain (DARC-ECD1-Mut), which is no longer recognized by the anti-DARC Nb (fig. S3), were cloned into the pGEX-5 plasmid (GE Healthcare). For protein expression, BL21 competent *E. coli* (New England Biolabs) was transformed with pMal-C2x-P18, the empty pMal-C2x plasmid (MBP alone), and pGEX-5-DARC-ECD1 as well as with pGEX-5-DARC-ECD1-Mut. Bacteria cultures were grown at 37°C until OD_{600nm} 0.5, and protein expression was carried out for 3 hours at 37°C with 0.1 mM isopropyl β-D-1-thiogalactopyranoside (IPTG) (Sigma-Aldrich). The bacteria pellets were resuspended in 50 mM tris and 500 mM NaCl at pH 7.2 and frozen at −80°C until further use. For protein purification, bacteria suspensions were thawed on ice and supplemented with EDTA-free cOmplete Protease Inhibitors (Roche) and with lysozyme (1 mg ml^{-1}) from chicken egg white (Sigma-Aldrich). Bacteria lysis was achieved by passing the cell suspensions through an EmulsiFlex-C5 high-pressure homogenizer (Avestin) three times at 4°C. Following centrifugation at 12,000*g*, the supernatants containing soluble proteins were subjected to a two-step purification process. MBP fusion proteins were first purified on amylose resin (New England Biolabs), whereas GST fusion proteins were purified on Glutathione Sepharose 4 Fast Flow (GE healthcare) according to the manufacturer's instructions. Purified proteins were then passed through a Superdex 200 10/300 GL gel filtration column (GE Healthcare) in phosphate-buffered saline (PBS) (Gibco) at pH 7.2. Double-purified proteins were snap-frozen in liquid nitrogen and stored at −80°C.

BMFP cloning, expression, and purification

The DNA sequence ORF BFRF3 encoding for P18 was recoded and optimized for *E. coli* codon usage (Integrated DNA Technology) to allow maximal expression in *E. coli*–based systems. The P18FL recoded sequence and the truncated fragment (P18F2, P18F3, and P18F4) sequences were cloned into a pet28a-derived plasmid (Novagen) to express C-terminal His-tagged proteins.

The anti-human CD20 (huCD20) V_H and V_L sequences of $scFv_{2H7}$ were obtained from the sequences of an anti-human CD28 x anti-huCD20 bispecific scFv antibody (clone r2820) (GenBank, AJ937362) and synthesized according to the following orientation: V_H-$(GGGGS)_3$-V_L. The DNA sequences of Nb-αDARC and $scFv_{2H7}$ were inserted between the Nhe I and Nco I restriction sites of Pet28a-NC (fig. S2). For each BMFP set, a construct comprising the binding moiety but lacking P18 was also generated.

For protein expression, *E. coli* SHuffle (New England Biolabs) was transformed with the different constructs. Bacteria cultures were induced with 0.2 mM IPTG at OD_{600nm} 0.8, and protein expression was carried out at 20°C for 16 hours. The bacteria pellets were resuspended in 50 mM tris and 500 mM NaCl at pH 7.2, and the samples were then frozen at −80°C until further use. For protein purification, bacteria suspensions were thawed on ice and supplemented with EDTA-free cOmplete Protease Inhibitors (Roche) and with lysozyme (1 mg ml^{-1}) from chicken egg white (Sigma-Aldrich). Bacteria lysis was achieved by passing the cell suspensions through an EmulsiFlex-C5 high-pressure homogenizer (Avestin) three times at 4°C. Following centrifugation at 12,000*g*, the supernatants containing soluble proteins were subjected to a two-step purification process. His-tagged proteins were first purified on Ni-NTA Superflow columns (Qiagen) according to the manufacturer's instructions and then passed through a Superdex 200 10/300 GL gel filtration column (GE Healthcare) in PBS at pH 7.2. Purified proteins were snap-frozen in liquid nitrogen and stored at −80°C.

Blood samples

Whole-blood samples were collected at the Etablissement Français du Sang (EFS)–Cabanel, Paris, France (convention number CCPSLUNT-N°12/EFS/135). RBCs and plasma samples were recovered after centrifugation of whole blood at 300*g* for 10 min. When required, complement inactivation was achieved by heating plasma samples at 56°C for 30 min. $DARC^+$ RBCs from individuals with the FY^{a+}/FY^{b+} genotype were obtained from a reference panel provided by the Centre National de Référence pour les Groupes Sanguins, Paris, France.

Cell lines

The marmoset B95-8 cells that produce infectious EBV particles, the human lymphoblastoid RAJI B cells (ECACC), and the human

monocytic leukemia THP1 cells (ECACC) were cultured in RPMI 1640 (Gibco), 2 mM glutamine (Gibco), 10% heat-inactivated fetal bovine serum (FBS) (D. Dutcher), and penicillin-streptomycin (100 U/ml) at 37°C and 5% CO_2. EL4-WT (ECACC) and EL4-huCD20 (provided by J. Golay, Bergamo, Italy) cells were maintained in Dulbecco's modified Eagle's medium (Gibco) supplemented with 2 mM glutamine (Gibco), 20% FBS, and penicillin-streptomycin (100 U/ml) at 37°C and 5% CO_2.

SPR studies of the binding of anti-DARC BMFPs to recombinant DARC-ECD1

Interactions between the anti-DARC BMFPs and DARC were studied by SPR, using a Biacore X100 instrument (GE Healthcare). All experiments were performed in HBS-EP (Hepes buffer saline EDTA surfactant P20) buffer (GE Healthcare) at 25°C. For studying the binding of Nb-αDARC, Nb-αDARC-P18F2, Nb-αDARC-P18F3, and Nb-αDARC-P18F4 to DARC, DARC-ECD1 was immobilized on the analysis Fc2 channel of a CM5 chip (GE Healthcare) by amine coupling, whereas DARC-ECD1-Mut was immobilized on the reference channel Fc1. Both channels were then blocked with 1 M ethanolamine-HCl (pH 8.5). BMFPs were injected at 30 μl min^{-1} in dilution series (0.1 to 125 μM) over the coated chips. Between the injections, the chip surface was regenerated with two injections of 15 μl of 10 mM HCl (pH 2.0). The specific binding responses to the molecular targets were obtained by subtracting the response given by the analytes on Fc2 with the response on Fc1. The kinetic sensorgrams were fitted to a global 1:1 interaction Langmuir model, and the k_{off} and k_{on} values were calculated using the manufacturer's software (Biacore X100 Evaluation version 2.0).

Immune recognition of BMFPs by anti-P18 IgG–containing human plasma

Ninety-six–well ultrahigh-binding flat-bottom microtiter plates (Immulon 4HBX) were coated overnight at 4°C with 100 μl of anti-DARC or anti-huCD20 BMFPs at 1 μg ml^{-1} in PBS. Plates were then washed three times with 200 μl of PBS and blocked for 1 hour at room temperature (RT) with 100 μl of PBS 1% BSA (Sigma-Aldrich). After removing the blocking solution, threefold serial dilutions (1/2 to 1/354,294) of human plasma were added into the wells and incubated for 1 hour at RT. Plates were then washed three times with PBS. One hundred microliters of AffiniPure $F(ab')_2$ fragment donkey anti-human IgG (Fcγ) horseradish peroxidase–conjugated antibody (Jackson ImmunoResearch) diluted 1/4000 in PBS 1% BSA was added to each well and incubated for 45 min at RT. Plates were then washed three times with PBS, and 100 μl of TMB (3,3′,5,5′-tetramethylbenzidine) substrate (Bio-Rad) was added per well. Absorbance was measured at 655 nm on an iMARK microplate absorbance reader (Bio-Rad). Data (OD_{655nm}) were plotted and subjected to four-parameter logistic regression curve fitting.

Binding of BMFPs to native molecular targets

Target cells (2.5×10^5) (RBCs, RAJI cells, EL4-WT, or EL4-huCD20 cells depending on the BMFPs tested) were distributed in a 96-well, round-bottom, polystyrene microplate (Corning, 3798) precoated with PBS 1% BSA for 1 hour at RT. To prevent nonspecific binding, cells were incubated with PBS 1% BSA for 1 hour at 4°C. Cells were then pelleted by centrifugation at 300*g* for 3 min at 4°C and resuspended in 100 μl of PBS 1% BSA containing BMFPs at various concentrations. Following 1 hour of incubation at 4°C, cells were washed three times with 200 μl of PBS 1% BSA and resuspended in 100 μl of PBS 1% BSA containing 0.5 μg of purified mouse anti-$(H)_5$ (Penta-His) (Qiagen). After 45 min, cells were washed three times with 200 μl of PBS 1% BSA and resuspended in 100 μl of PBS 1% BSA containing AffiniPure $F(ab')_2$ fragment goat anti-mouse IgG (H+L), phycoerythrin (PE)–conjugated (1/100) (Jackson ImmunoResearch). After 45 min, cells were washed three times with 200 μl of PBS and subjected to flow cytometry analysis in the presence of TO-PRO-3 (Molecular Probes) diluted 1/10,000. Data acquisition was performed using a BD FACSCanto II flow cytometer (Becton Dickinson). Target cell gating was performed on the basis of morphological features using the forward and side scatters. TO-PRO-3–positive dead cells were excluded. Data were then analyzed in FlowJo 8.1 (Tree Star Inc.) software.

Anti-DARC BMFP–mediated opsonization of RBCs

Target cells (2.5×10^5 RBCs) were distributed in a 96-well plate precoated with PBS 1% BSA for 1 hour at RT. To prevent nonspecific binding, RBCs were incubated with PBS 1% BSA for 1 hour at 4°C. Cells were then pelleted and resuspended in 100 μl of PBS 1% BSA containing 9.6 nM Nb-αDARC-P18F3. Following 1 hour of incubation at 4°C, RBCs were washed three times with 200 μl of PBS 1% BSA and resuspended in 100 μl of human plasma pools diluted from 1/5 to 1/10,240 in PBS 1% BSA. After 1 hour, cells were washed three times with 200 μl of PBS 1% BSA and resuspended in 100 μl of PBS 1% BSA containing PE-conjugated AffiniPure $F(ab')_2$ fragment donkey anti-human IgG (Fc) (1/100) (Jackson ImmunoResearch). After 45 min, RBCs were washed three times with 200 μl of PBS and subjected to flow cytometry.

Antibody-dependent phagocytosis

THP1 cells were differentiated into M0 macrophage-like cells with PMA (Sigma-Aldrich). Briefly, THP1 cells were seeded in 12-well plates (7.5×10^5 cells per well) and incubated for 48 hours at 37°C and 5% CO_2 in complete medium supplemented with PMA (20 ng/ml). FY^+ human RBCs were stained with CFSE (Thermo Fisher Scientific) according to the manufacturer's instructions. Stained RBCs were incubated for 1 hour at RT with Nb-αDARC-18F3 or with Nb-αDARC at saturating concentrations in PBS 1% BSA and subsequently with human plasma pools diluted 1/10 in PBS 1% BSA. Opsonized RBCs were then incubated for 3 hours at 37°C and 5% CO_2 with THP1-derived macrophage-like cells at an effector/target cell ratio of 1/100. After coincubation, nonphagocytized RBCs were lysed with RBC lysis buffer (ChemCruz), and macrophage-like cells were subjected to flow cytometry analysis in the presence of TO-PRO-3 diluted 1/10,000. $CFSE^+$ macrophage-like cells were considered as cells having phagocytized at least one RBC.

Activation of complement cascade

Target RAJI cells (2.5×10^5) were distributed in a 96-well plate precoated with PBS 1% BSA for 1 hour at RT. To prevent nonspecific binding, cells were incubated with PBS 1% BSA for 1 hour at 4°C. Cells were then pelleted and resuspended in 100 μl of PBS 1% BSA containing $scFv_{2H7}$-P18F3 or $scFv_{2H7}$ at 0.48 μM. Following 1 hour of incubation at 4°C, cells were washed three times with 200 μl of PBS 1% BSA and resuspended in 100 μl of undiluted heat-inactivated (56°C, 30 min) or untreated plasma. After a 1-hour incubation at 37°C, cells were washed three times with 200 μl of PBS

1% BSA and resuspended in 100 µl of PBS 1% BSA containing purified mouse (IgG2a, κ) anti–C5b-9 + C5b-8 (aE11) (20 µg ml^{-1}) or rabbit polyclonal anti–C5b-9 (25 µg ml^{-1}) (Abcam). After 45 min at 4°C, cells were washed three times with 200 µl of PBS 1% BSA and resuspended in 100 µl of PBS 1% BSA containing APC-conjugated goat anti-mouse IgG (Fcγ fragment–specific) (1/100) or PE-conjugated donkey anti-rabbit IgG (H+L) (1/100) (Jackson ImmunoResearch). After 20 min at 4°C, cells were washed three times with 200 µl of PBS and subjected to flow cytometry analysis.

Triggering of early events of ADCC

$ScFv_{2H7}$-P18F3–mediated triggering of early events of ADCC was monitored using the reporter Bioassay Core Kit (Promega) according to the manufacturer's instructions. Target RAJI cells (12,500) were distributed in a 96-well plate precoated with PBS 1% BSA for 1 hour at RT. To prevent nonspecific binding, cells were incubated with PBS 1% BSA for 1 hour at 4°C. Cells were then pelleted and resuspended in 100 µl of PBS 1% BSA containing $scFv_{2H7}$-P18F3 or $scFv_{2H7}$ at 0.48 µM. Following 1 hour of incubation at 4°C, cells were washed three times with 200 µl of PBS 1% BSA and resuspended in ADCC assay buffer containing heat-inactivated (56°C, 30 min) human plasma at different dilutions. Effector $FcγRIII^+$ Jurkat cells (75,000) were added into each well. Plates were incubated at 37°C and 5% CO_2 for 6 hours. Plates were then equilibrated at 25°C for 15 min before the introduction of Bio-Glo into each well. Plates were left for 30 min at 25°C before luminescence reading on a PerkinElmer Victor 2030 plate reader.

Generation of mouse anti-P18FL antibodies

Six-week-old female BALB/cByJ mice (Charles River) were immunized with MBP-P18FL following four subcutaneous injections at days 0, 14, 28, and 42 [25 µg of MBP-P18FL per injection in combination with Freund's complete adjuvant (FCA) at day 0 and incomplete Freund adjuvant (IFA) at days 14, 28, and 42]. Blood samples were collected at day −1 (preimmune serum) and at day 52 (immune serum). Mice immunization was performed by Biotem (Grenoble, France, ISO9001:2015; certificate FR0536014-1). Animal immunization was executed in strict accordance with good animal practices, following the European Union (EU) animal welfare legislation and after approval of the INSERM and Biotem ethical committees.

Anti-CD20 BMFP–mediated opsonization of RAJI and EL4-huCD20 cells

RAJI or EL4-huCD20 target cells (2.5×10^5) were distributed in a 96-well plate precoated with PBS 1% BSA for 1 hour at RT. To prevent nonspecific binding, cells were incubated with PBS 1% BSA for 1 hour at 4°C. Cells were then pelleted and resuspended in 100 µl of PBS 1% BSA containing 0.48 µM $scFv_{2H7}$-P18F3. Following 1 hour of incubation at 4°C, cells were washed three times with 200 µl of PBS 1% BSA and resuspended in 100 µl of individual mouse serum (diluted from 1/10) in PBS 1%. After 1 hour, cells were washed three times with 200 µl of PBS 1% BSA and resuspended in 100 µl of PBS 1% BSA containing PE-conjugated AffiniPure $F(ab')_2$ fragment goat anti-mouse IgG (H+L) (1/100) (Jackson ImmunoResearch). After 45 min, cells were washed three times with 200 µl of PBS and subjected to flow cytometry analysis in the presence of TO-PRO-3 diluted 1/10,000 to discriminate live and dead cells.

In vivo tumor therapy

Six-week-old female immunocompetent C57Bl/6 mice (Charles River) were immunized with MBP-P18FL by three subcutaneous injections at days 0, 14, and 28 (25 µg of MBP-P18FL per injection in combination with FCA at day 0 and IFA at days 14 and 28). Mice were then intravenously inoculated in the tail vein on day 0 with 2.5×10^5 EL4-huCD20 cells per mouse [in 200 µl of PBS (pH 7.4)], 56 days (experiment 1; Fig. 6C), or 10 days (experiment 2; Fig. 6D) after the last immunization with MBP-P18FL. $ScFv_{2H7}$-P18F3 therapy was given as four intraperitoneal injections of 57 µg per mouse [in 200 µl of PBS (pH 7.4)] on days 1, 4, 7, and 10. Another group of mice received 46 µg of $scFv_{2H7}$ [in 200 µl of PBS (pH 7.4)] according to the same injection schedules. Animals were followed daily for up to 120 days. Mice were euthanized as soon as one of the following clinical criteria appeared: presence of tumor on palpation, hindquarter paralysis, prostration, weight loss, hair bristling, and abnormal abdominal swelling. Blood samples were collected 2 days before and 15 days after the start of the treatment. Animal experimentation was performed in compliance with the guidelines from the EU (EU guideline on animal experiments, European Directive #2010/63/EU) and the national charter on ethics in animal experiments and was approved by the local Charles Darwin Ethics Committee in Animal Experiments, Paris, France (authorization number 01530.02).

Analysis of anti–$scFv_{2H7}$-P18F3 IgG subclasses

Ninety-six–well ultrahigh-binding flat-bottom microtiter plates (Immulon 4HBX) were coated overnight at 4°C with 100 µl of $scFv_{2H7}$-P18F3 at 1 µg/ml in PBS. Plates were then washed three times with 200 µl of PBS and blocked for 1 hour at RT with 100 µl of PBS 1% BSA (Sigma-Aldrich). After removing the blocking solution, individual mouse sera (1/5) in PBS 1% BSA were added into the wells and incubated for 1 hour at RT. Plates were then washed three times with PBS. One hundred microliters of alkaline phosphatase–conjugated goat anti-mouse IgG1, IgG2a, IgG2b, or IgG3 (Jackson ImmunoResearch) diluted 1/4000 in PBS 1% BSA was added to each well and incubated for 45 min at RT. Plates were then washed three times with PBS, and 100 µl of TMB substrate (Bio-Rad) was added per well. Absorbance was measured at 415 nm on an iMARK microplate absorbance reader (Bio-Rad).

Statistical analysis

The Prism software was used to analyze data, draw graphs, and perform statistical analyses. The specific type of test (Mann-Whitney test, Dunn's multiple comparison test, and log-rank Mantel-Cox test) used to analyze the data is mentioned in the figure legends. *P* values of ≤0.05 were regarded as statistically significant (*$P \leq 0.05$, **$P \leq 0.01$, ***$P \leq 0.001$, and ****$P \leq 0.0001$).

Antibodies

All antibodies used in the study are listed in table S1.

SUPPLEMENTARY MATERIALS

Supplementary material for this article is available at https://science.org/doi/10.1126/sciadv.abl4363

REFERENCES AND NOTES

1. R.-M. Lu, Y.-C. Hwang, I.-J. Liu, C.-C. Lee, H.-Z. Tsai, H.-J. Li, H.-C. Wu, Development of therapeutic antibodies for the treatment of diseases. *J. Biomed. Sci.* **27**, 1 (2020).
2. M. L. Chiu, D. R. Goulet, A. Teplyakov, G. L. Gilliland, Antibody structure and function: The basis for engineering therapeutics. *Antibodies* **8**, 55 (2019).

3. T. H. Kang, S. T. Jung, Boosting therapeutic potency of antibodies by taming Fc domain functions. *Exp. Mol. Med.* **51**, 1–9 (2019).
4. X. Wang, M. Mathieu, R. J. Brezski, IgG Fc engineering to modulate antibody effector functions. *Protein Cell* **9**, 63–73 (2018).
5. M. J. Gramer, J. J. Eckblad, R. Donahue, J. Brown, C. Shultz, K. Vickerman, P. Priem, E. T. J. van den Bremer, J. Gerritsen, P. H. C. van Berkel, Modulation of antibody galactosylation through feeding of uridine, manganese chloride, and galactose. *Biotechnol. Bioeng.* **108**, 1591–1602 (2011).
6. C. A. Diebolder, F. J. Beurskens, R. N. de Jong, R. I. Koning, K. Strumane, M. A. Lindorfer, M. Voorhorst, D. Ugurlar, S. Rosati, A. J. R. Heck, J. G. J. van de Winkel, I. A. Wilson, A. J. Koster, R. P. Taylor, E. O. Saphire, D. R. Burton, J. Schuurman, P. Gros, P. W. H. I. Parren, Complement is activated by IgG hexamers assembled at the cell surface. *Science* **343**, 1260–1263 (2014).
7. R. L. Shields, J. Lai, R. Keck, L. Y. O'Connell, K. Hong, Y. G. Meng, S. H. A. Weikert, L. G. Presta, Lack of fucose on human IgG1 N-linked oligosaccharide improves binding to human FcγRIII and antibody-dependent cellular toxicity. *J. Biol. Chem.* **277**, 26733–26740 (2002).
8. F. Mimoto, T. Igawa, T. Kuramochi, H. Katada, S. Kadono, T. Kamikawa, M. Shida-Kawazoe, K. Hattori, Novel asymmetrically engineered antibody Fc variant with superior FcγR binding affinity and specificity compared with afucosylated Fc variant. *MAbs* **5**, 229–236 (2013).
9. S. Sibéril, C. de Romeuf, N. Bihoreau, N. Fernandez, J.-L. Meterreau, A. Regenman, E. Nony, C. Gaucher, A. Glacet, S. Jorieux, P. Klein, M. P. Hogarth, W.-H. Fridman, D. Bourel, R. Béliard, J.-L. Teillaud, Selection of a human anti-RhD monoclonal antibody for therapeutic use: Impact of IgG glycosylation on activating and inhibitory Fc gamma R functions. *Clin. Immunol.* **118**, 170–179 (2006).
10. R. Beliard, T. Waegemans, D. Notelet, L. Massad, F. Dhainaut, C. de Romeuf, E. Guemas, W. Haazen, D. Bourel, J.-L. Teillaud, J.-F. Prost, A human anti-D monoclonal antibody selected for enhanced FcγRIII engagement clears RhD^+ autologous red cells in human volunteers as efficiently as polyclonal anti-D antibodies. *Br. J. Haematol.* **141**, 109–119 (2008).
11. J. O. Richards, S. Karki, G. A. Lazar, H. Chen, W. Dang, J. R. Desjarlais, Optimization of antibody binding to FcgammaRIIa enhances macrophage phagocytosis of tumor cells. *Mol. Cancer Ther.* **7**, 2517–2527 (2008).
12. W. F. Dall'Acqua, P. A. Kiener, H. Wu, Properties of human IgG1s engineered for enhanced binding to the neonatal Fc receptor (FcRn). *J. Biol. Chem.* **281**, 23514–23524 (2006).
13. G. J. Robbie, R. Criste, W. F. Dall'acqua, K. Jensen, N. K. Patel, G. A. Losonsky, M. P. Griffin, A novel investigational Fc-modified humanized monoclonal antibody, motavizumab-YTE, has an extended half-life in healthy adults. *Antimicrob. Agents Chemother.* **57**, 6147–6153 (2013).
14. J. J. M. A. Hendrikx, J. B. A. G. Haanen, E. E. Voest, J. H. M. Schellens, A. D. R. Huitema, J. H. Beijnen, Fixed dosing of monoclonal antibodies in oncology. *Oncologist* **22**, 1212–1221 (2017).
15. L. S. Young, A. B. Rickinson, Epstein–Barr virus: 40 years on. *Nat. Rev. Cancer* **4**, 757–768 (2004).
16. G. J. Babcock, L. L. Decker, M. Volk, D. A. Thorley-Lawson, EBV persistence in memory B cells in vivo. *Immunity* **9**, 395–404 (1998).
17. D. A. Thorley-Lawson, in *Epstein Barr Virus Volume 1*, C. Münz, Ed. (Current Topics in Microbiology and Immunology, Springer International Publishing, 2015), vol. 390, pp. 151–209.
18. S. Ogolla, I. I. Daud, A. S. Asito, O. P. Sumba, C. Ouma, J. Vulule, J. M. Middeldorp, A. E. Dent, S. Mehta, R. Rochford, Reduced transplacental transfer of a subset of Epstein-Barr virus-specific antibodies to neonates of mothers infected with plasmodium falciparum malaria during pregnancy. *Clin. Vaccine Immunol.* **22**, 1197–1205 (2015).
19. H. Kaplon, J. M. Reichert, Antibodies to watch in 2021. *MAbs* **13**, 1860476 (2021).
20. N. S. Merle, S. E. Church, V. Fremeaux-Bacchi, L. T. Roumenina, Complement system part I—Molecular mechanisms of activation and regulation. *Front. Immunol.* **6**, 262 (2015).
21. N. S. Merle, R. Noe, L. Halbwachs-Mecarelli, V. Fremeaux-Bacchi, L. T. Roumenina, Complement system part II: Role in immunity. *Front. Immunol.* **6**, 257 (2015).
22. F. Nimmerjahn, J. V. Ravetch, Fcγ receptors as regulators of immune responses. *Nat. Rev. Immunol.* **8**, 34–47 (2008).
23. P. M. Hogarth, G. A. Pietersz, Fc receptor-targeted therapies for the treatment of inflammation, cancer and beyond. *Nat. Rev. Drug Discov.* **11**, 311–331 (2012).
24. R. M. Anthony, F. Nimmerjahn, D. J. Ashline, V. N. Reinhold, J. C. Paulson, J. V. Ravetch, Recapitulation of IVIG anti-inflammatory activity with a recombinant IgG Fc. *Science* **320**, 373–376 (2008).
25. R. Abès, E. Gélizé, W. H. Fridman, J.-L. Teillaud, Long-lasting antitumor protection by anti-CD20 antibody through cellular immune response. *Blood* **116**, 926–934 (2010).
26. D. J. DiLillo, J. V. Ravetch, Differential Fc-receptor engagement drives an anti-tumor vaccinal effect. *Cell* **161**, 1035–1045 (2015).
27. R. Horuk, The Duffy antigen receptor for chemokines DARC/ACKR1. *Front. Immunol.* **6**, 279 (2015).
28. D. Smolarek, C. Hattab, G. Hassanzadeh-Ghassabeh, S. Cochet, C. Gutiérrez, A. G. de Brevern, R. Udomsangpetch, J. Picot, M. Grodecka, K. Wasniowska, S. Muyldermans, Y. Colin, C. Le Van Kim, M. Czerwinski, O. Bertrand, A recombinant dromedary antibody fragment (VHH or nanobody) directed against human Duffy antigen receptor for chemokines. *Cell. Mol. Life Sci.* **67**, 3371–3387 (2010).
29. J. Lobstein, C. A. Emrich, C. Jeans, M. Faulkner, P. Riggs, M. Berkmen, SHuffle, a novel *Escherichia coli* protein expression strain capable of correctly folding disulfide bonded proteins in its cytoplasm. *Microb. Cell Fact.* **11**, 753 (2012).
30. E. Uribe-Querol, C. Rosales, Phagocytosis: Our current understanding of a universal biological process. *Front. Immunol.* **11**, 1066 (2020).
31. S. Tsuchiya, M. Yamabe, Y. Yamaguchi, Y. Kobayashi, T. Konno, K. Tada, Establishment and characterization of a human acute monocytic leukemia cell line (THP-1). *Int. J. Cancer* **26**, 171–176 (1980).
32. A. Y. Liu, R. R. Robinson, E. D. Murray Jr., J. A. Ledbetter, I. Hellström, K. E. Hellström, Production of a mouse-human chimeric monoclonal antibody to CD20 with potent Fc-dependent biologic activity. *J. Immunol.* **139**, 3521–3526 (1987).
33. B. S. Parekh, E. Berger, S. Sibley, S. Cahya, L. Xiao, M. A. LaCerte, P. Vaillancourt, S. Wooden, D. Gately, Development and validation of an antibody-dependent cell-mediated cytotoxicity-reporter gene assay. *MAbs* **4**, 310–318 (2012).
34. N. Di Gaetano, E. Cittera, R. Nota, A. Vecchi, V. Grieco, E. Scanziani, M. Botto, M. Introna, J. Golay, Complement activation determines the therapeutic activity of rituximab in vivo. *J. Immunol.* **171**, 1581–1587 (2003).
35. A. Chêne, S. Gangnard, A. Guadall, H. Ginisty, O. Leroy, N. Havelange, N. K. Viebig, B. Gamain, Preclinical immunogenicity and safety of the cGMP-grade placental malaria vaccine PRIMVAC. *EBioMedicine* **42**, 145–156 (2019).
36. S. B. Sirima, L. Richert, A. Chêne, A. T. Konate, C. Campion, S. Dechavanne, J.-P. Semblat, N. Benhamouda, M. Bahuaud, P. Loulergue, A. Ouédraogo, I. Nébié, M. Kabore, D. Kargougou, A. Barry, S. M. Ouattara, V. Boilet, F. Allais, G. Roguet, N. Havelange, E. Lopez-Perez, A. Kuppers, E. Konaté, C. Roussillon, M. Kanté, L. Belarbi, A. Diarra, N. Henry, I. Soulama, A. Ouédraogo, H. Esperou, O. Leroy, F. Batteux, E. Tartour, N. K. Viebig, R. Thiebaut, O. Launay, B. Gamain, PRIMVAC vaccine adjuvanted with Alhydrogel or GLA-SE to prevent placental malaria: A first-in-human, randomised, double-blind, placebo-controlled study. *Lancet Infect. Dis.* **20**, 585–597 (2020).
37. W. M. van Grunsven, W. J. Spaan, J. M. Middeldorp, Localization and diagnostic application of immunodominant domains of the BFRF3-encoded Epstein-Barr virus capsid protein. *J. Infect. Dis.* **170**, 13–19 (1994).
38. J. M. L. Casan, J. Wong, M. J. Northcott, S. Opat, Anti-CD20 monoclonal antibodies: Reviewing a revolution. *Hum. Vaccin. Immunother.* **14**, 2820–2841 (2018).
39. G. Salles, M. Barrett, R. Foà, J. Maurer, S. O'Brien, N. Valente, M. Wenger, D. G. Maloney, Rituximab in B-cell hematologic malignancies: A review of 20 years of clinical experience. *Adv. Ther.* **34**, 2232–2273 (2017).
40. C. de Romeuf, C.-A. Dutertre, M. Le Garff-Tavernier, N. Fournier, C. Gaucher, A. Glacet, S. Jorieux, N. Bihoreau, C. K. Behrens, R. Béliard, V. Vieillard, B. Cazin, D. Bourel, J.-F. Prost, J.-L. Teillaud, H. Merle-Béral, Chronic lymphocytic leukaemia cells are efficiently killed by an anti-CD20 monoclonal antibody selected for improved engagement of FcgammaRIIIA/CD16. *Br. J. Haematol.* **140**, 635–643 (2008).
41. Z. N. Soe, D. Allsup, The use of ofatumumab in the treatment of B-cell malignancies. *Future Oncol.* **13**, 2611–2628 (2017).
42. A. Prica, M. Crump, Improving CD20 antibody therapy: Obinutuzumab in lymphoproliferative disorders. *Leuk. Lymphoma* **60**, 573–582 (2019).
43. J. Du, H. Wang, C. Zhong, B. Peng, M. Zhang, B. Li, S. Hou, Y. Guo, J. Ding, Crystal structure of chimeric antibody C2H7 Fab in complex with a CD20 peptide. *Mol. Immunol.* **45**, 2861–2868 (2008).
44. R. Wang, S. Xiang, Y. Feng, S. Srinivas, Y. Zhang, M. Lin, S. Wang, Engineering production of functional scFv antibody in *E. coli* by co-expressing the molecule chaperone Skp. *Front. Cell. Infect. Microbiol.* **3**, 72 (2013).
45. A. Sarker, A. S. Rathore, R. D. Gupta, Evaluation of scFv protein recovery from *E. coli* by in vitro refolding and mild solubilization process. *Microb. Cell Fact.* **18**, 5 (2019).
46. M. Arbabi-Ghahroudi, J. Tanha, R. MacKenzie, Prokaryotic expression of antibodies. *Cancer Metastasis Rev.* **24**, 501–519 (2005).
47. I. Jovčevska, S. Muyldermans, The therapeutic potential of nanobodies. *BioDrugs* **34**, 11–26 (2020).
48. J. Golay, E. Cittera, N. Di Gaetano, M. Manganini, M. Mosca, M. Nebuloni, N. van Rooijen, L. Vago, M. Introna, The role of complement in the therapeutic activity of rituximab in a murine B lymphoma model homing in lymph nodes. *Haematologica* **91**, 176–183 (2006).
49. G. Miller, T. Shope, D. Coope, L. Waters, J. Pagano, G. Bornkamm, W. Henle, Lymphoma in cotton-top marmosets after inoculation with Epstein-Barr virus: Tumor incidence, histologic spectrum antibody responses, demonstration of viral DNA, and characterization of viruses. *J. Exp. Med.* **145**, 948–967 (1977).
50. M. Yajima, K.-I. Imadome, A. Nakagawa, S. Watanabe, K. Terashima, H. Nakamura, M. Ito, N. Shimizu, M. Honda, N. Yamamoto, S. Fujiwara, A new humanized mouse model of Epstein-Barr virus infection that reproduces persistent infection, lymphoproliferative disorder, and cell-mediated and humoral immune responses. *J Infect Dis* **198**, 673–682 (2008).

51. S. Fujiwara, K.-I. Imadome, M. Takei, Modeling EBV infection and pathogenesis in new-generation humanized mice. *Exp. Mol. Med.* **47**, e135 (2015).
52. R. Akkina, New generation humanized mice for virus research: Comparative aspects and future prospects. *Virology* **435**, 14–28 (2013).
53. C. Deligne, A. Metidji, W.-H. Fridman, J.-L. Teillaud, Anti-CD20 therapy induces a memory Th1 response through the IFN-γ/IL-12 axis and prevents protumor regulatory T-cell expansion in mice. *Leukemia* **29**, 947–957 (2015).
54. P. Bruhns, F. Jönsson, Mouse and human FcR effector functions. *Immunol. Rev.* **268**, 25–51 (2015).
55. A. E. Coghill, C. Proietti, Z. Liu, L. Krause, J. Bethony, L. Prokunina-Olsson, A. Obajemu, F. Nkrumah, R. J. Biggar, K. Bhatia, A. Hildesheim, D. L. Doolan, S. M. Mbulaiteye, The association between the comprehensive Epstein-Barr virus serologic profile and endemic burkitt lymphoma. *Cancer Epidemiol. Biomarkers Prev.* **29**, 57–62 (2020).
56. D. Donati, E. Espmark, F. Kironde, E. K. Mbidde, M. Kamya, A. Lundkvist, M. Wahlgren, M. T. Bejarano, K. I. Falk, Clearance of circulating Epstein-Barr virus DNA in children with acute malaria after antimalaria treatment. *J Infect Dis* **193**, 971–977 (2006).
57. J. E. Gold, R. A. Okyay, W. E. Licht, D. J. Hurley, Investigation of long COVID prevalence and its relationship to Epstein-Barr virus reactivation. *Pathogens* **10**, 763 (2021).
58. European Medicines Agency; www.ema.europa.eu/en.

Acknowledgments: We are thankful to D. Goossens, Z. Gouveia, and N. Josseaume for providing reagents, to M. Marin and S. Peltier for technical assistance, and to G. Milon for inspiring discussions. **Funding:** This work was supported by SATT IDF-Innov, Paris, France (to B.G. and A.C.); Institut National de la Santé et de la Recherche Médicale (INSERM), France (to B.G. and A.C.); and Institut National de la Transfusion Sanguine (INTS), Paris, France (to B.G. and A.C.). **Author contributions:** Conceptualization: B.G., O.B., S.G., J.-L.T., and A.C. Investigation: C.B., N.E.R., B.K.D., C.-E.P., A.D., J.C., J.-P.S., and A.C. Supervision: B.G., J.-L.T., and A.C. Writing—original draft: B.G., J.-L.T., and A.C. All authors critically reviewed and validated the submitted version of the manuscript. **Competing interests:** B.G., S.G., and A.C. are inventors on a patent application related to this work filed by Institut National de la Transfusion Sanguine, Centre National de la Recherche Scientifique (CNRS), INSERM, Université de Paris (no. WO2017103020A1, filed 25 December 2015, published 22 June 2017). The authors declare that they have no other competing interests. **Data and materials availability:** All data needed to evaluate the conclusions in the paper are present in the paper and/or the Supplementary Materials.

Submitted 13 July 2021
Accepted 17 December 2021
Published 11 February 2022
10.1126/sciadv.abl4363

ScienceAdvances

BMFPs, a versatile therapeutic tool for redirecting a preexisting Epstein-Barr virus antibody response toward defined target cells

Benoît GamainCarine BrousseNathan E. RaineyBéré K. DialloClara-Eva PaquereauAlexandra DesramesJolita CeputyteJean-Philippe SemblatOlivier BertrandStéphane GangnardJean-Luc TeillaudArnaud Chêne

Sci. Adv., 8 (6), eabl4363. • DOI: 10.1126/sciadv.abl4363